The unusual structure of Ruminococcin C1 antimicrobial peptide confers clinical properties

Clarisse Roblin, Steve Chiumento, Olivier Bornet, Matthieu Nouailler, Christina S. Müller, Katy Jeannot, Christian Basset, Sylvie Kieffer-Jaquinod, Yohann Couté, Stéphane Torelli, et al.

The unusual structure of Ruminococcin C1 antimicrobial peptide confers clinical properties

Clarisse Roblin[1,2†], Steve Chiumento[3†], Olivier Bornet[4*], Matthieu Nouailler[5], Christina S. Müller[6], Katy Jeannot[7,8], Christian Basset[3], Sylvie Kieffer-Jaquinod[9], Yohann Couté[9], Stéphane Torelli[3], Laurent Le Pape[3], Volker Schünemann[6], Hamza Olleik[1], Bruno De La Villeon[10], Philippe Sockeel[10], Eric Di Pasquale[11], Cendrine Nicoletti[1], Nicolas Vidal[12], Leonora Poljak[13], Olga Iranzo[1], Thierry Giardina[1], Michel Fons[14], Estelle Devillard[2], Patrice Polard[13], Marc Maresca[1], Josette Perrier[1], Mohamed Atta[3], Françoise Guerlesquin[5], Mickael Lafond[1*], Victor Duarte[3*]

[1]Aix-Marseille Univ, CNRS, Centrale Marseille, iSm2, 13013, Marseille, France.

[2]ADISSEO France SAS, Centre d'Expertise et de Recherche en Nutrition, 03600, Commentry, France.

[3]Univ. Grenoble Alpes, CEA, IRIG, CBM, CNRS UMR5249, 38054, Grenoble, France.

[4]NMR platform, Institut de Microbiologie de la Méditerranée, CNRS, Aix-Marseille Université, 13009, Marseille, France.

[5]Laboratoire d'Ingénierie des Systèmes Macromoléculaires, UMR7255, Institut de Microbiologie de la Méditerranée, CNRS, Aix-Marseille Université, 13009, Marseille, France.

[6]Fachbreich Physik, Technische Universität Kaiserslautern, Erwin-Schrödinger-Str. 56, 67663, Kaiserslautern, Germany.

[7]Centre National de Référence de la Résistance aux Antibiotiques, Laboratoire de Bactériologie, Centre Hospitalier Universitaire de Besançon, 25030, Besançon, France.

[8]UMR 6249 Chrono-Environnement, UFR Santé, Université de Bourgogne-Franche-Comté, 25030, Besançon, France.

[9]Univ. Grenoble Alpes, CEA, Inserm, IRIG, BGE, 38054, Grenoble, France.

[10]Departement of Digestive, Endocrine and Metabolic Surgery, Hôpital Laveran, Military Health Service, 13013 Marseille, France.

[11]Aix Marseille Univ, Faculté de Médecine, Institut de NeuroPhysioPathologie, 13397 Marseille, France.

[12]Yelen Analytics, 10 bd tempête, 13820 Ensues la Redonne, France.

[13]Laboratoire de Microbiologie et de Génétique Moléculaires, Centre de Biologie Intégrative, Université de Toulouse, CNRS, UPS, Toulouse, France.

[14]Laboratoire de Bioénergétique et Ingénierie des protéines, UMR 7281, Institut de Microbiologie de la Méditerranée, CNRS, Aix-Marseille Université, 13009, Marseille, France.

* Correspondence to: bornet@imm.cnrs.fr; mickael.lafond@univ-amu.fr; victor.duarte@cea.fr

† The following authors contributed equally to this work: Clarisse Roblin & Steve Chiumento

Radical SAM enzyme, RiPP, sactipeptide, *Ruminococcus gnavus*, antibiotic

The emergence of superbugs developing resistance to antibiotics and the resurgence of microbial infections have led scientists to start an antimicrobial arms race. In this context, we have previously identified an active RiPP, the Ruminococcin C1, naturally produced by *Ruminococcus gnavus* E1, a symbiont of the healthy human intestinal microbiota. This RiPP, subclassified as a sactipeptide, requires the host digestive system to become active against pathogenic Clostridia and multidrug resistant strains. Here, we report its unique compact structure on the basis of four intramolecular thioether bridges with reversed stereochemistry introduced post-translationally by a specific radical-SAM sactisynthase. This structure confers to the Ruminococcin C1 important clinical properties including stability to digestive conditions and physicochemical treatments, a higher affinity for bacteria than simulated intestinal epithelium, a valuable activity at therapeutic doses on a range of clinical pathogens, mediated by energy resources disruption and finally safety for human gut tissues.

Significance

Since the discovery of penicillin, humans have widely developed and used antibiotics to protect themselves from microbial infections. However, the intensive use of these compounds has led to the emergence of pathogens resistant to all classes of antibiotics. This major public health threat has led scientists to find new molecules with different structures and modes of action to overcome resistance phenomena. A promising alternative concerns bacteriocins secreted by certain bacteria. Of a peptidic nature, their ribosomal synthesis differentiates them from conventional antibiotics. The recently identified RumC1 antimicrobial peptide presents a remarkable bactericidal activity for multi-drug resistant strains. Added to this efficacy, RumC1 is not toxic against a number of human cell lines and is safe for human gut tissues.

INTRODUCTION

Ribosomally synthesized and Post-translationally modified Peptides (RiPPs) are an important group of compounds that have stimulated research interest, notably as natural antimicrobial agents with bacteriocins (1). During RiPPs biogenesis, a precursor peptide composed of at least a leader and a core sequence is synthesized by the ribosome. The core peptide is modified by tailoring enzymes and then the leader sequence is cleaved by one or two peptidases to produce the final active product (1–4). Among the RiPPs, sactipeptides (Sulfur-to-alpha carbon thioether cross-linked peptides) are a subgroup that has emerged in recent years (5–7). Despite spectacular soaring made with genomic tools, the sactipeptide subclass is currently limited to only seven members. They include subtilosin A (SboA) (8, 9), thurincin H (10), the sporulation killing factor (SkfA) (11), thuricin CD that consists of two peptides, Trn-α and Trn-β (12), thuricin Z or huazacin (13, 14) and the recently characterized Ruminococcin C1 (RumC1) (15, 16).

The precise mechanistic details of sactipeptide cross-link formation are not fully understood. However, from a chemical point of view, the thioether bonds in these natural products are distinct from those of the well-studied lanthipeptides, such as nisin, in which they are formed between a Cys residue and a β-carbon of a dehydrated Thr/Ser residue (17). In contrast to the two-step redox neutral mechanism used for the maturation of lanthipeptides, radical-SAM sactisynthase enzymes introduce chemically equivalent thioether bonds by a one-step radical-based mechanism (5–7). The enzymes within this superfamily contain the canonical $CysX_3CysX_2Cys$ motif, that binds the radical-SAM $[4Fe\text{-}4S]^{2+/1+}$ cluster (referred to as the RS cluster), in which the fourth, unique iron, is used to bind S-adenosylmethionine (SAM) cofactor (18). In its reduced state, the $[4Fe\text{-}4S]^{1+}$ cluster catalyzes the reductive cleavage of SAM to generate a 5′-deoxyadenosyl radical (5'-Ado•). This radical abstracts a H- atom from the cognate substrate to initiate catalysis (18). In the case of the characterized radical-SAM enzymes involved in the sactipeptide biosynthesis, H-atom abstraction was shown to occur from the α-carbon of the acceptor residue (5–7). A survey of available structural and functional data indicate that all radical-SAM enzymes involved in the sactipeptides biosynthesis contain a C-terminal extension appended to the radical-SAM domain called SPASM/Twitch domain that houses additional [4Fe-4S] clusters (19, 20). In contrast to the Twitch domains, which bind only one additional cluster, SPASM domains present a conserved cysteine-rich motif that coordinates two additional iron-sulfur clusters. The role of these clusters remains to be clarified, but it was suggested that they possibly interact with the substrate during catalysis or may also be implicated in electrons transfer (5–7, 21).

Among the seven sactipeptides reported to date, four are structurally characterized (SboA, thurincin H, Trn-α and Trn-β) and all of them have been purified from the genus

Bacillus. SboA is a cyclic peptide with three thioether bridges involving two phenylalanines and one threonine. Trn-α, Trn-β and thurincin H are not cyclic, they present three and four thioether bridges, respectively. One common feature of SboA, Trn-α, Trn-β and thurincin H is that they all present Cys residues in the N-terminal half and the corresponding partners at the C-terminal part, a property that folds the peptide in a single hairpin-shaped form with the hydrophobic residues facing outwards as showed by the available structures (8–10, 12, 22). Sequence analysis of the last identified sactipeptide, namely RumC1, suggests a new fold. Indeed, one pair of cysteines is located at the N-terminal part of the sequence while the other one is in the C-terminal end (Fig. 1A). Recent data on the characterization of mature RumC1 by mass spectrometry, strongly suggests that the thioether network folds the peptide in a double hairpin like structure that differs from the currently reported ones (16). Furthermore, sactipeptides and by extension antimicrobial peptides (including RiPPs but not only) have emerged as a potential trove of new weapons and alternatives to conventional antibiotics to fight multidrug-resistant (MDR) bacteria. However, their clinical use remains a challenge due to high cost of production, sensitivity to physiological or manufacturing conditions, as well as toxicity for human tissues (23, 24). In this context, we previously showed that RumC1 has a potent activity against Gram positive bacteria and is harmless for human cells (16). Obviously, the next step was to study RumC1 in a clinical context and to address the above-mentioned reasons that prevent antimicrobial peptides from being considered for pharmaceutical development.

In this work, we sought to determine the three-dimensional structure of RumC1. The rapid and large-scale production of ^{13}C- and ^{15}N-labelled mature RumC1, by heterologous expression in *Escherichia coli* (16, 25), allowed extensive nuclear magnetic resonance (NMR) analyses to solve the structure of RumC1 and to propose the thioether network stereochemistry. In the meantime, combined EPR and Mössbauer spectroscopies enabled us to characterize the Fe-S clusters in RumMc1 sactisynthase. Finally, we point out that the fold of RumC1 confers resistance to physical, chemical and digestive constraints, features essential for consideration in pharmaceuticals. The clinical properties of RumC1 also covers activity against clinical pathogens, including resistant strains, maintained in a mammalian environment and mediated through energy resources depletion, without any impact to human tissues.

Results

RumC1 sactipeptide displays a double hairpin-like structure. The two-dimensional [^{1}H, ^{15}N] HSQC spectrum of RumC1 is well-resolved with 39 peptide amide peaks out of 42 expected, thus attesting for the folding of the protein (fig. S1). No NH peaks were observed for residues C26, G27

and N28, probably due to fast amide exchange with the solvent and/or high flexibility of the region. We assigned the backbone carbon, nitrogen and proton resonances using a combined strategy of sequential residue correlations based on HNCACB, CBCA(CO)NH, HNCA, HN(CO)CA, HNCO, HN(CA)CO triple resonance experiments, and through-space nOe connectivities using 2D [^{1}H, ^{1}H] NOESY, 3D [^{1}H, ^{15}N, ^{1}H] and 3D [^{1}H, ^{13}C, ^{1}H] NOESY experiments. NMR studies of Subtilosin A, Thuricin CD and Thurincin H, by Vederas *et. al.* have shown that cysteine sulfur to α-carbon thioether linkages induce a 10 to 15 ppm downfield shift for the α-carbon atoms of bridged residues (8–10, 12, 22). Moreover, through-space nOe interactions were observed between the β-protons of cysteines and the amide proton (NH) of modified residues (8–10, 12, 22). In the same manner, we have demonstrated that RumC1 contains four sulfur to α-carbon thioether cross-links between Cys3 and Asn16, Cys5 and Ala12, Cys22 and Lys42, and Cys26 and Arg34 (16). Since there are four thioether bridges, each can adopt one of the two possible configurations at the α-carbon atom (L or D). Consequently, 16 stereoisomers must be considered to establish the three-dimensional structure of RumC1. Calculations for all 16 stereoisomers were carried out using the CYANA software and seven rounds performed on each stereoisomer using the same NMR restraints file (26). The structural statistics and constraint violations (table S1) allowed to identify the stereoisomer with the D stereochemistry at Ala12 (α-S), Asn16 (α-S), Arg34 (α-S) and Lys42 (α-S) as a representative structure given: i) the absence of thioether bridge constraint violations, ii) the great number of nOe connectivities used in the structure calculation, iii) the lowest average target function value and a low root mean square deviation (*rmsd*). To improve the structure of the DDDD stereoisomer, an additional refinement step by returning to the NOESY spectra to eliminate the ambiguities found during the structure calculation by the CYANA software was added. The resulting structural statistics of the 20 conformers for the DDDD isomer of RumC1 are summarized in table S2. The backbones of the 20 lowest target function value conformers for the DDDD isomer of RumC1 superimpose quite well with a *rmsd* value of 0.81 Å for the backbone (Fig. 1B). The three-dimensional structure of RumC1 is thus composed on both sides by two α-helices and in the middle by a 2-stranded parallel β-sheet fragment and the whole stiffened by four cysteine sulfur to α-carbon thioether cross-links (Fig. 1C).

The electrostatic surface potentials present an overall positive charge (Fig. 1D) and the surface hydrophobicity of the DDDD stereoisomer shows a majority of hydrophilic residues (Fig. 1E). The compact three-dimensional solution structure of RumC1 reveals a new sactipeptide fold and by extension a new antimicrobial peptide fold (fig. S2A). Four sulfur to α-carbon thioether bridges with a DDDD stereochemistry have been already reported for thurincin H (10). However, the

presence of an additional 2-stranded parallel β-sheet fragment in the middle of RumC1 induces a new fold, thus resulting in a different location of the thioether crosslinks (fig. S2, B-E) (9, 10, 22).

Expression, purification and characterization of the RumMc1 sactisynthase. RumMc1 is predicted to contain accessory Fe-S clusters, in addition to the RS cluster, thus we decided to co-express the *rumMc1* gene with the pDB1282 plasmid, which encodes for a set of proteins involved in iron-sulfur cluster biogenesis (IscS, IscU, IscA, HscB, HscA and Fdx) (27). After the final step of anaerobic purification, the purity was evaluated by SDS-PAGE to be over 95% (fig. S3). As expected, the holo-RumMc1 protein was dark brown in color and the iron titration revealed, on average, ten metal centers per monomer. In good agreement, the UV-vis spectrum of holo-RumMc1 suggests the presence of [4Fe-4S] clusters (Fig. 2A, solid line). Mössbauer spectroscopy on ^{57}Fe-enriched oxidized holo-RumMc1was then used to deeply investigate the nature of the Fe-S clusters. The experimental spectrum recorded at T = 77 K (dashed line) could be simulated (red line) with three components **1**, **2** and **3** in a 2:1:1 ratio (Fig. 2B). **1** and **2** are characterized by similar isomer shifts (δ) with $\delta = 0.42$ mms^{-1} for **1** and $\delta = 0.44$ mms^{-1} for **2** while the quadrupole splitting (ΔE_q) varies with $\Delta E_q = 0.98$ mms^{-1} for **1** and $\Delta E_q = 1.30$ mms^{-1} for **2**. These values are in a typical range for $Fe^{2,5+}$ ions in a diamagnetic $[4Fe\text{-}4S]^{2+}$ cluster (28–30). This is supported by simulations of the spectra recorded at T = 4.2 K in external fields of B = 0.1 T and B = 5 T (fig. S4, A and B) based on the spin Hamilton formalism assuming a total spin of S = 0. The 2:1 ratio suggests that holo-RumMc1 contains three $[4Fe\text{-}4S]^{2+}$ clusters. This is supported by the sequence alignment of RumMc1 with other related proteins that contain conserved cysteine residues localized at the C-terminal half of the protein (fig. S5). Hence, we can conclude that **1** represents 8 $Fe^{2,5+}$ ions in the same tetrahedral sulfur environment belonging to two $[4Fe\text{-}4S]^{2+}$ clusters while **2** corresponds to four indistinguishable $Fe^{2,5+}$ ions present in the single $[4Fe\text{-}4S]^{2+}$ cluster supposed to contain the SAM-binding iron site (RS-cluster). The difference in ΔE_q between **1** and **2** points to a slightly different distribution of electron density. **3** is characterized by $\delta = 0.33$ mms^{-1} and $\Delta E_q = 0.49$ mms^{-1} typical for Fe^{3+} high spin (S = 5/2) in a tetrahedral sulfur environment (28). This component was adequately simulated (fig. S4A, with an external magnetic field) by combining contributions from three distinct, but antiferromagnetically coupled Fe^{3+} centers, thus resulting in a global S = 1/2 spin state as described for a paramagnetic $[3Fe\text{-}4S]^{1+}$ cluster (31, 32). The respective hyperfine parameters are characteristic for $[3Fe\text{-}4S]^{1+}$ clusters (fig. S4B) (31, 32). Upon addition of dithionite on the holo-RumMc1, the absorption decreased over the entire 310-420 nm range as expected for the conversion of the S = 0 $[4Fe\text{-}4S]^{2+}$ chromophore to the S = 1/2 $[4Fe\text{-}4S]^{1+}$ level (Fig. 2A, dashed line). This reduced form has been investigated by X-band EPR spectroscopy in order to gain

insights into the individual features of the three [4Fe-4S] clusters involved. The experimental EPR spectrum of holo-RumMc1 is extremely rich, suggesting the presence of multiple S = 1/2 [4Fe-4S]$^{1+}$ clusters (fig. 2C, black line). It was satisfactorily simulated considering the three following sets of g-tensors [2.034, 1.913, 1.870] (**A**), [2.050, 1.937, 1.902] (**B**) and [2.074, 1.932, 1.885] (**C**) (Fig. 2, C and E). Addition of the natural SAM cofactor then induced a substantial change in the spectrum that was well simulated with four sets of g-tensors [2.034, 1.910, 1.860] (**A**), [2.049, 1.937, 1.904] (**B**), [2.073, 1.932, 1.885] (**C**) and [2.076, 1.930, 1.852] (**A'**) instead of three (Fig. 2, D and E). As the contribution of **A** has to be lowered to achieve a reliable simulation, these experiments support that **A** originates from the RS cluster while **B** and **C** rely to two additional clusters. The new component **A'** was assigned to the amount of the RS cluster, which is bond to the SAM as previously described (33).

Efficient maturation of RumC1: both the leader and the core sequences are crucial. Here we sought to gain insights into the features of RumC1 that are required for its efficient maturation by RumMc1. It is established that the post-translational modification of RiPPs is an event that is dependent on the presence of the leader peptide (2). For example, in the case of the sactipeptide subclass, Marahiel and co-workers have shown that AlbA failed to transform a variant of the SboA peptide without its leader sequence in a mature sactipeptide (34). We investigated the maturation of RumC1 by the way of an *in vitro* assay in the presence of RumMc1, the SAM cofactor and dithionite as an external electron source. These experiments were performed with a full-length RumC1 precursor peptide, a leader less variant of 44 amino acids (RumC1-44) and a third condition in which the leader sequence and the core peptide were dissociated but both present in the solution (RumC1-44-LS). The reaction mixtures were analyzed by LC-MS to detect the formation of thioether bonds within the three substrates (fig. S6). Since the full maturation of RumC1 leads to the formation of four thioether bonds, the percentages of maturation (fig. S6A) account for the species that present a loss of 8 Da in mass compared to the unmodified substrate. The data clearly indicate that only the RumC1 peptide is fully modified, both RumC1-44 and RumC1-44-LS led to less than one and ten percent of species with four thioether linkages, respectively (fig. S6, A and B). It has to be noted that attempts to yield mature peptides form the latter two substrates lead mainly to a mixture of peptides harboring partial maturation with 2 and 3 thioether bonds (fig. S6, C and D). In good agreement with the lack of maturation of RumC1-44 during the *in vitro* enzymatic assay, we also observed that no mature peptide is obtained when this leader less form of RumC1 is produced *in vivo* using the heterologous expression and maturation protocol in *E. coli* (fig. S7A).

In contrast to the sactipeptides identified so far, the thioether connectivity in RumC1 folds the peptide in a double hairpin like structure. Sequence alignments of the five RumC isoforms shows a strictly conserved Gly18/Pro19 motif in the loop region between the two hairpins (16). We therefore sought to determine whether this motif is necessary for inducing a turn in the sequence and allowing the peptide maturation by RumMc1. For this, we replaced the Gly18/Pro19 motif by Ala18/Ala19. LC-MS analysis of the heterologously expressed Ala18/Ala19 RumC1 variant clearly demonstrate the lack of maturation thus suggesting that the loop alteration in RumC1 may disturb substrate-enzyme interactions that are crucial for the formation of the thioether network (fig. S7B). As reported by Grove and coworkers for CteA (21), these results suggest that the binding of RumC1 by RumMc1 involves determinants from both the leader and the core sequences.

The compact structure confers a high stability to RumC1. Studies have proven the potent activity of sactipeptides (12, 35), however there is a lack of evidence showing that they possess the physiochemical properties necessary for *in vivo* administration and, from an applied point of view, for pharmaceutical development (35). Consequently, we assayed the tolerance of RumC1 to such properties. RumC1 showed no loss of activity when exposed to acidic or basic pH from 2 to 11 (Fig. 3A). Furthermore, RumC1 was resistant to 70 and 100°C for up to 1 hour and more than 15 minutes respectively, meaning that RumC1 possesses the intrinsic thermal resistance that are required for drug formulation processes (Fig. 3B). Because of their sensitivities to enzymatic digestion or to physiological salts concentrations and blood enzymes, the administration of antimicrobial peptides by oral route and/or systemic injection is limited. Interestingly, the activity of RumC1 wasn't impaired by salts concentrations higher than 150 mM for NaCl and 2 mM for $MgCl_2$ (Fig. 3C), which are considered as physiological saline conditions. Likewise, incubation in human serum at 37°C up to 24 hours did not affect the activity of RumC1 (Fig. 3D). RumC1 was finally treated with pepsin at pH 2.5 for 2 hours at 37°C, and with pancreatin at pH 6.5 for 5 hours at 37°C in order to mimic the human gastric and intestinal compartments, respectively. RumC1 showed no loss of activity and its integrity was revealed by MS analysis after these treatments whereas the lanthipeptide nisin used as a positive control for pancreatin activity showed reduced antimicrobial potency (Fig. 3E, fig. S8, A and B). Pepsin activity was confirmed as well by hydrolysis of Bovine Serum Albumine (BSA) (fig. S8A). Therefore, the thioether network leading to a compact structure of RumC1 confers to the sactipeptide high resistance to physico-chemical treatments and to the physiological but harsh conditions encountered in blood or in the digestive tract after systemic or oral administration.

RumC1 is able to act on a simulated infected intestinal epithelium. Many studies on antimicrobial peptides show their direct activity on bacterial cultures, without considering their efficiency in a mammalian environment, such as an infected epithelium. Indeed, antimicrobial peptides can act on bacteria but can also insert into eukaryotic cells or merely bind to their surface (24, 36), which could cause a partial loss of activity against extracellular pathogens. On the contrary, some peptides have higher affinity for bacterial cells than host cells (37). Therefore, we assayed the potency of RumC1 against *Bacillus cereus*, an aerotolerant human intestinal opportunistic pathogen, on simulated gut epitheliums using Caco2 and T84 cells as models of human small intestinal and colonic epithelium, respectively. *B. cereus* was able to grow on untreated monolayers of Caco2 and T84 whereas treatment with RumC1 was effective to clear the infection (fig. S9). The MIC of RumC1 against *B. cereus* was measured in the eukaryotic cell line culture medium in the presence or the absence of human intestinal cells. The MIC value did not increase in the presence of intestinal cells when RumC1 was added 30 min before, concomitantly or 30 min after the bacterial cells (Fig. 4A). Indeed, no loss of activity was detected as well when *B. cereus* was allowed to colonize the epithelium for 30 min before adding RumC1 (Fig. 4A). Therefore, it appears that RumC1 has a preferential affinity for bacterial cells rather than host cells. Finally, these results suggest that the physiological environment of the two cell lines did not affect significantly the activity of RumC1.

RumC1 displays a potent activity against Gram-positive pathogenic clinical isolates. We previously showed that RumC1 is active against a broad range of Gram-positive bacteria including resistant and multi-resistant strains (16), but focusing only on collection strains. In order to evaluate the potentiality of RumC1 being considered for pharmaceutical development, we investigated its activity against Gram-positive strains isolated in a clinical context from humans or animals (i.e. broiler chickens). As RumC1 was first identified for its anti- *Clostridium perfringens* activity (16, 38, 39), we measured for the first time the MIC of the sactipeptide against a large panel of *C. perfringens* clinical isolates (Fig. 4B). RumC1 was active under the micromolar range (between 0.4 and 0.8 µM) on all the ten strains tested. In comparison with the reference molecules, usually used to eradicate *C. perfringens*, RumC1 showed a higher activity than metronidazole (12 to 23 µM) and an activity similar to vancomycin (0.2 to 0.4 µM). Interestingly, in a livestock context, RumC1 was not only active against the CP24 *C. perfringens* strain isolated from a healthy broiler chicken, but also against strains isolated from animals suffering from dysbiosis or necrotic enteritis, respectively CP56 and CP60 (40). In addition, RumC was also active against *C. perfringens* strains isolated from humans suffering from bacteremia ($n=6$) (Fig. 4B).

Then, we studied the effect of RumC1 on another main intestinal pathogen from the *Clostridium* genus, *Clostridium difficile*. RumC1 showed activity against collection and clinical strains of *C. difficile* with lower MIC (0.3 to 0.6 µM) than two of the most common antibiotics used for *C. difficile* intestinal infections (CDI), i.e. metronidazole (1.5 µM) and vancomycin (0.3 to 0.7 µM) (Fig. 4B). Moreover, RumC1 is also efficient at the micromolar range against other intestinal pathogens (clinical and collection strains) of main importance such as *Listeria monocytogenes, B. cereus, Enterococcus faecalis* and *Enterococcus faecium* including strains resistant to amoxicillin and/or vancomycin (Fig. 4B). Beside its activity against pathogens causing gut infections, RumC1 is also active against a clinical *Streptococcus pneumoniae* strain at a low MIC (0.3 µM), a pathogen responsible of multiple types of infection (including respiratory tract infection, meningitis and septicemia) (Fig. 4B).

The killing mechanism of RumC1 involves energy resource shortage. Unlike many bacteriocins RumC1 does not have a pore forming action (16), we therefore investigated its effects on the main macromolecules synthesis pathways usually targeted by antibiotics. *C. perfringens* cells were exposed to RumC1 and the synthesis of DNA, RNA, proteins and peptidoglycan were followed by measuring the incorporation of radio-labelled precursors. Remarkably, RumC1 was able to inhibit the synthesis pathways of the four macromolecules with efficacies similar to conventional antibiotics targeting each of these pathways (Fig. 5A). As these synthesis pathways are all energy-dependent, we assayed the potency of RumC1 to break such energy resources. Thus, we measured by bioluminescent assay the ATP released by *C. perfringens* cells in the extracellular medium, and then lysed cells to derive the intracellular ATP content (Fig 5B). Upon treatment with RumC1 for 15 min, outer ATP was not increased compared to cells untreated whereas inner ATP decreased in a dose-dependent manner. Treatment with nisin, a pore-forming bacteriocin led to drastic increase of outer ATP whereas metronidazole does not impact ATP synthesis pathway. Since the synthesis of DNA, RNA, proteins and peptidoglycan accounts for the consumption of approximately 70 % of the total ATP content of bacteria, their observed inhibition is likely linked to ATP depletion and therefore the specificity of RumC1 could be related to an inhibition of the ATP synthesis pathway (41).

Integrity of human tissues treated with RumC1. We previously reported that RumC1 was a safe new antimicrobial peptide because of its lack of *in vitro* toxicity on gastric and intestinal cell lines culture (16). To further characterize the safety of RumC1, we assayed the toxicity of the sactipeptide *ex vivo,* directly on human ileocecal tissues. Intestinal explants were isolated from unaffected area

of ileocecal resection from two patients diagnosed with intestinal carcinoma and were incubated with RumC1 at 100 µM or the detergent CTAB at 300 µM for 4 hours. Control and RumC1 exposed human intestinal explants displayed normal tissue organization with normal crypt and villosity lengths and no sign of epithelial desquamation or erosion, in accordance with data we obtained previously *in vitro* on human intestinal cell lines. Conversely, exposure to CTAB, used as positive control of tissue damages, caused important lesions to the human intestinal epithelium with cell desquamation and shortening of the crypts and villosities (Fig. 6).

Discussion

In this study, we elucidated the three-dimensional structure of mature Ruminococcin C1 from *Ruminococcus gnavus* E1. NMR experiments clearly showed that the thioether network of RumC1, involving four sulfur to α-carbon bridges, folds the peptide into a double hairpin-like motif, which differs from the currently reported structures within the sactipeptide family. By extension, the fold not described so far includes two-stranded parallel β-sheet into the core enclosed between two parallel α-helixes. In contrast to a recent report by Berteau *et al.*, where the residues involved in the thioether bridges were identified to be L-configurated, after hydrolysis and derivatization (15), here we found that the stereoisomers that fits best with the NMR data featured D-configurations at Ala12, Asn16, Arg34 and Lys42. RumC1 has a global positive charge at physiological pH and displays a constrained and rigid backbone structure that presents a mostly hydrophilic surface unlike sactipeptides with known structure presenting mostly hydrophobic surface. These sactipeptides, like most of the bacteriocins that target Gram-positive strains, have a pore-forming mode of action. Despite an overall cationic charge, RumC1 is unable to insert into lipids extracts most likely due to its hydrophilic surface and exerts probably an intracellular mode of action reaching one or more specific targets by active transport.

The double hairpin-like structure of RumC1 provides stability to pH and high-temperatures, which could facilitate pharmaceutical manufacturing processes. We also showed that RumC1 is resistant to digestive proteolytic conditions, most likely because the sites of cleavage are protected by the four thioether bonds and the tridimensional folding of the peptide. Many RiPPs including sactipeptides, such as Subtilosin A and Thuricin CD, are not resistant to both pepsin and pancreatic proteases (42, 43), implying that the original folding of RumC1 offers additional protection. Moreover, RumC1 is also resistant to physiological salts conditions as well as to human serum, which can both be detrimental for an exogenous compound. Based on these considerations, we followed our investigations of RumC1 in a preclinical context. The first step was to ensure that RumC1 could cure infections in the mammalian environment. Therefore, we treated with RumC1

a *B. cereus* infected simulated epitheliums. RumC1 remained active at very low doses, exactly at the same level as the MIC obtained in the absence of eukaryotic cells. This observation confirms the stronger affinity of RumC1 for bacterial versus host cells, and the specific primary function of RumC1 as antibiotic compound. Then we checked that RumC1 has potent activity on Gram-positive clinical pathogens and not only on collections strains. RumC1 showed strong activity under the micromolar range toward *Clostridia* pathogens from both human and animal origins. The measured MICs are equivalent to vancomycin, one of the reference antibiotics used in therapy against these pathogens, and lower than metronidazole, another reference antibiotic known to generate resistance (16). Therefore, the use of RumC1 to treat infections caused by *C. perfringens* or *C. difficile* should be considered. Indeed, from a livestock point of view, *C. perfringens* can cause necrotic enteritis, which is one of the most common infection in broiler chickens with mortality rates as high as 50% and resulting in dehydration, lesions on intestinal mucosa or other organs like the liver, spleen, heart or kidneys (44). On the other hand, *C. difficile* is a major human pathogen causing nosocomial infections, community-associated diarrhea and is responsible of 250,000 intestinal infections per year in the US, associated with a mortality rate of 15 to 20%. In 2019, *C. difficile* has been classified by the Centre for Diseases Control and Prevention as an urgent threat for which new antimicrobials are needed (45, 46). In the same line, RumC1 is active against amoxicillin and vancomycin resistant *E. faecium*, registered on all priority lists of human pathogens for which new antimicrobials are urgently needed. It is registered by the CDC as a serious concern that requires prompt action and by the WHO on the "antibiotic-resistant priority pathogens" as high concern. *E. faecium* is also pointed by the Infectious Diseases Society of America (IDSA) across the "ESKAPE pathogens" list of bacteria, which includes *Enterococcus faecium, Staphylococcus aureus, Klebsiella pneumoniae, Acinetobacter baumannii, Pseudomonas aeruginosa* and *Enterobacter* spp., (47) for its ability to escape the effects of the commonly used antibiotics through evolutionarily developed mechanisms of resistance (48). *E. faecium,* characterized by drug resistance mechanisms, commonly causes life-threatening nosocomial infections amongst critically ill and immunocompromised individuals. Consequently, it is important to note that RumC1 is particularly active against this pathogen with a MIC of 1,2 µM, thus it could be considered as a potential therapeutic solution. In the case of *S. pneumoniae,* with a prevalence of 1.2 million of infections per year in the US, leading to its inclusion into the CDC and the WHO lists of priority pathogens, the use of RumC1 with a MIC of 300 nM may also be relevant. It should be noted that RumC1 is a broad-spectrum anti-Gram-positive molecule directed against resistant anaerobic and aerobic clinical pathogens, which is rare in the antibiotics market with a few exceptions such as vancomycin, thus enhancing its clinical potential. Moreover, we showed that RumC1 inhibits the

synthesis of macromolecules including DNA, RNA, proteins or peptidoglycan and the production of ATP. At this stage, since the main biosynthetic pathways are inhibited, it is conceivable that RumC1 applies its antimicrobial activity intracellularly through a non-specific mechanism, or conversely, targeting specifically ATP synthases and thus disrupting all necessary energy resources, such as bedaquiline, the only antibiotic currently on the market targeting ATP synthases but used only for the treatment of infections caused by Mycobacterium (49). Otherwise, we have previously identified that the phenotype induced by RumC1 treatment resembles the one induced by metronidazole in *C. perfringens* (16). However, we have shown here that metronidazole only inhibits DNA synthesis and, to a lesser extent, protein synthesis. Metronidazole is known to impact DNA synthesis and repair systems, and most likely inhibits the activity of the strictly ATP-dependent ribonucleotide reductase by modulating the redox state of cells, but its precise mechanism remains elusive (50). Here we suggest that the phenotypic similarities induced by RumC1 and metronidazole might arise from a DNA synthesis inhibition and possibly other common events, although they certainly do not share the same mechanism. Therefore, further in-depth investigations are needed to resolve the potentially unique intracellular mode of action of RumC1. Finally, we followed our preclinical studies by assessing the safety of RumC1 on gut tissues directly sourced from patients. RumC1 did not induce epithelial lesions at a dose about a hundred times higher than the effective antimicrobial dose. This observation could be expected as humans have been exposed to RumC1 through evolution as this peptide is produced by a symbiotic bacterium present in the gut microbiota of healthy adults. Overall, RumC1 encompass properties essential for a drug candidate to cure intestinal infections, especially since i) it can be administrated by oral route, ii) it is active in the intestinal epithelium environment, iii) RumC1 shows activity at therapeutic doses against clinical intestinal resistant pathogens, and finally iv) since it is safe for gut tissues. Only few AMPs meet all the conditions that are necessary for reaching the marketing step, i.e. respecting the conditions of stability, presenting activity under physiological conditions (including in the presence of eukaryotic cells), owning antimicrobial effect against clinical pathogens at very low doses including resistant or MDR, and finally retaining safety for human cells and tissues. It is interesting to note that RumC1 fulfils all these conditions, except one remaining bottleneck for the industrial scale use, which concerns the cost of production. RumC-like synthetic molecule development could be addressed to solve this concern and highlight the great potential of this original sactipeptide.

Materials and Methods

Detailed descriptions of materials and methods, including expression, purification of (^{13}C, ^{15}N)-labelled mature RumC1, NMR studies, structure calculations, EPR and Mössbauer analyses of RumMc1, stability assays of RumC1 and MIC determinations are given in *SI Appendix*.

Supporting Information

Supplementary figures Fig. S1 to Fig. S9 as well as Tables S1 and S2 are provided in *SI Appendix*.

Data Availability

All data needed to evaluate the conclusions in the paper are present in the paper and the *SI Appendix*. All of the peak lists and the complete ^{1}H, ^{13}C and ^{15}N backbone and side chain chemical shift assignments of RumC1 have been deposited into the Biological Magnetic Resonance Databank (http://www.bmrb.wisc.edu) under ascension code 50027. Coordinates of the twenty conformations of DDDD stereoisomer of RumC1 have been deposited into the PDB under ascension code 6T33.

ACKNOWLEDGMENTS. We would like to thank Pr. Richard Ducatelle and Pr. Filip Van Immerseel from UGent for providing us with clinical isolates of *C. perfringens* from broiler chickens. We would also like to thank Pr. Lhousseine Touqui for scientific advising. Finally, we would like to thank the people from the AVB platform (iSm2 CNRS UMR 7313, Marseille). This study was supported by grants from the French National Agency for Research ("Agence Nationale de la Recherche") through the "Projet de Recherche Collaboratif" (*RUMBA project,* ANR-15-CE21-0020), the "Investissement d'Avenir Infrastructures Nationales en Biologie et Santé" programme (*ProFI project,* ANR-10-INBS-08) and partial financial support from the Labex ARCANE and CBH-EUR-GS (ANR-17-EURE-0003). We are grateful to Adisseo France company and the Association Nationale Recherche Technologie (ANRT) for funding the doctoral fellowship of C.R. entitled "Bacteriocins RumC, a novel antimicrobial peptide family as alternative to conventional antibiotics." This grant numbered *Convention Industrielle de Formation par la RecherchE* (CIFRE) no. 2016/0657 runs from 1 March 2017 to 1 March 2020. VS and CSM. acknowledge the support of the German Science Foundation (DFG) within SPP 1927 (SCHU 1251/17-1, 2).

Author contributions: CR, SC, KJ and CB performed the *in vitro* assays for RumC1, RumMc1 and were involved in interpreting the data and writing the manuscript; OB and MN performed the RumC1 structural analysis by RMN; CSM and VS performed the Mössbauer analyses on RumMc1 and wrote the corresponding parts; ST and LLP performed the EPR analysis on RumMc1; SKJ and

YC performed nanoLC-MS/MS characterizations; BDLV, PS, EDP, MM and CN performed the chirurgical biopsy, the human explant treatment, the cytotoxicity assays and the microscopy analysis; HO, NV and LP were involved in biosynthetic pathways and ATP assays; OI performed the peptide chemical synthesis; TG, MF and ED were involved in study design; PP, JP, MA, FG, ML and VD conceptualized the study, designed experiments, interpreted the data and wrote the manuscript.

Competing interests: The authors declare that they have no competing interests.

References

1. P. G. Arnison, *et al.*, Ribosomally synthesized and post-translationally modified peptide natural products: overview and recommendations for a universal nomenclature. *Nat. Prod. Rep.* **30**, 108–160 (2013).

2. T. J. Oman, W. A. van der Donk, Follow the leader: the use of leader peptides to guide natural product biosynthesis. *Nat. Chem. Biol.* **6**, 9–18 (2010).

3. G. A. Hudson, D. A. Mitchell, RiPP antibiotics: biosynthesis and engineering potential. *Curr. Opin. Microbiol.* **45**, 61–69 (2018).

4. J. R. Chekan, C. Ongpipattanakul, S. K. Nair, Steric complementarity directs sequence promiscuous leader binding in RiPP biosynthesis. *Proc. Natl. Acad. Sci.* **116**, 24049–24055 (2019).

5. N. Mahanta, G. A. Hudson, D. A. Mitchell, Radical S-Adenosylmethionine Enzymes Involved in RiPP Biosynthesis. *Biochemistry* **56**, 5229–5244 (2017).

6. A. Benjdia, C. Balty, O. Berteau, Radical SAM Enzymes in the Biosynthesis of Ribosomally Synthesized and Post-translationally Modified Peptides (RiPPs). *Front. Chem.* **5**, 87 (2017).

7. L. Flühe, M. A. Marahiel, Radical S-adenosylmethionine enzyme catalyzed thioether bond formation in sactipeptide biosynthesis. *Curr. Opin. Chem. Biol.* **17**, 605–612 (2013).

8. K. Kawulka, *et al.*, Structure of Subtilosin A, an Antimicrobial Peptide from *Bacillus subtilis* with Unusual Posttranslational Modifications Linking Cysteine Sulfurs to α-Carbons of Phenylalanine and Threonine. *J. Am. Chem. Soc.* **125**, 4726–4727 (2003).

9. K. E. Kawulka, *et al.*, Structure of subtilosin A, a cyclic antimicrobial peptide from *Bacillus subtilis* with unusual sulfur to alpha-carbon cross-links: formation and reduction of alpha-thio-alpha-amino acid derivatives. *Biochemistry* **43**, 3385–3395 (2004).

10. C. S. Sit, M. J. van Belkum, R. T. McKay, R. W. Worobo, J. C. Vederas, The 3D Solution Structure of Thurincin H, a Bacteriocin with Four Sulfur to α-Carbon Crosslinks. *Angew. Chem. Int. Ed.* **50**, 8718–8721 (2011).

11. W.-T. Liu, *et al.*, Imaging mass spectrometry of intraspecies metabolic exchange revealed the cannibalistic factors of *Bacillus subtilis*. *Proc. Natl. Acad. Sci.* **107**, 16286–16290 (2010).

12. M. C. Rea, *et al.*, Thuricin CD, a posttranslationally modified bacteriocin with a narrow spectrum of activity against *Clostridium difficile*. *Proc. Natl. Acad. Sci. U. S. A.* **107**, 9352–9357 (2010).

13. T. Mo, *et al.*, Thuricin Z: A Narrow-Spectrum Sactibiotic that Targets the Cell Membrane. *Angew. Chem. Int. Ed Engl.* **58**, 18793–18797 (2019).

14. G. A. Hudson, *et al.*, Bioinformatic Mapping of Radical S-Adenosylmethionine-Dependent Ribosomally Synthesized and Post-Translationally Modified Peptides Identifies New Cα, Cβ, and Cγ-Linked Thioether-Containing Peptides. *J. Am. Chem. Soc.* **141**, 8228–8238 (2019).

15. C. Balty, *et al.*, Ruminococcin C, an anti-clostridial sactipeptide produced by a prominent member of the human microbiota *Ruminococcus gnavus*. *J. Biol. Chem.* **294**, 14512–14525 (2019).

16. S. Chiumento, *et al.*, Ruminococcin C, a promising antibiotic produced by a human gut symbiont. *Sci. Adv.* **5**, eaaw9969 (2019).

17. P. J. Knerr, W. A. van der Donk, Discovery, biosynthesis, and engineering of lantipeptides. *Annu. Rev. Biochem.* **81**, 479–505 (2012).

18. J. B. Broderick, B. R. Duffus, K. S. Duschene, E. M. Shepard, Radical S-Adenosylmethionine Enzymes. *Chem. Rev.* **114**, 4229–4317 (2014).

19. T. A. J. Grell, P. J. Goldman, C. L. Drennan, SPASM and Twitch Domains in *S* -Adenosylmethionine (SAM) Radical Enzymes. *J. Biol. Chem.* **290**, 3964–3971 (2015).

20. J. A. Latham, I. Barr, J. P. Klinman, At the confluence of ribosomally synthesized peptide modification and radical S-adenosylmethionine (SAM) enzymology. *J. Biol. Chem.* **292**, 16397–16405 (2017).

21. T. L. Grove, *et al.*, Structural Insights into Thioether Bond Formation in the Biosynthesis of Sactipeptides. *J. Am. Chem. Soc.* **139**, 11734–11744 (2017).

22. C. S. Sit, R. T. McKay, C. Hill, R. P. Ross, J. C. Vederas, The 3D structure of thuricin CD, a two-component bacteriocin with cysteine sulfur to α-carbon cross-links. *J. Am. Chem. Soc.* **133**, 7680–7683 (2011).

23. M. Mahlapuu, J. Håkansson, L. Ringstad, C. Björn, Antimicrobial Peptides: An Emerging Category of Therapeutic Agents. *Front. Cell. Infect. Microbiol.* **6** (2016).

24. W. Aoki, M. Ueda, Characterization of Antimicrobial Peptides toward the Development of Novel Antibiotics. *Pharm. Basel Switz.* **6**, 1055–1081 (2013).

25. P. M. Himes, S. E. Allen, S. Hwang, A. A. Bowers, Production of Sactipeptides in Escherichia coli: Probing the Substrate Promiscuity of Subtilosin A Biosynthesis. *ACS Chem. Biol.* **11**, 1737–1744 (2016).

26. P. Güntert, C. Mumenthaler, K. Wüthrich, Torsion angle dynamics for NMR structure calculation with the new program DYANA. *J. Mol. Biol.* **273**, 283–298 (1997).

27. R. M. Cicchillo, *et al.*, Lipoyl synthase requires two equivalents of S-adenosyl-L-methionine to synthesize one equivalent of lipoic acid. *Biochemistry* **43**, 6378–6386 (2004).

28. M.-E. Pandelia, N. D. Lanz, S. J. Booker, C. Krebs, Mössbauer spectroscopy of Fe/S proteins. *Biochim. Biophys. Acta* **1853**, 1395–1405 (2015).

29. P. Middleton, D. P. E. Dickson, C. E. Johnson, J. D. Rush, Interpretation of the Mössbauer Spectra of the Four-Iron Ferredoxin from *Bacillus stearothermophilus*. *Eur. J. Biochem.* **88**, 135–141 (1978).

30. G. Layer, *et al.*, Radical S-Adenosylmethionine Enzyme Coproporphyrinogen III Oxidase HemN. *J. Biol. Chem.* **280**, 29038–29046 (2005).

31. B. H. Huynh, *et al.*, On the active sites of the [NiFe] hydrogenase from *Desulfovibrio gigas.* Mössbauer and redox-titration studies. *J. Biol. Chem.* **262**, 795–800 (1987).

32. M. Teixeira, *et al.*, Redox intermediates of *Desulfovibrio gigas* [NiFe] hydrogenase generated under hydrogen. Mössbauer and EPR characterization of the metal centers. *J. Biol. Chem.* **264**, 16435–16450 (1989).

33. N. A. Bruender, J. Wilcoxen, R. D. Britt, V. Bandarian, Biochemical and Spectroscopic Characterization of a Radical S-Adenosyl-L-methionine Enzyme Involved in the Formation of a Peptide Thioether Cross-Link. *Biochemistry* **55**, 2122–2134 (2016).

34. L. Flühe, *et al.*, The radical SAM enzyme AlbA catalyzes thioether bond formation in subtilosin A. *Nat. Chem. Biol.* **8**, 350–357 (2012).

35. H. Mathur, M. C. Rea, P. D. Cotter, C. Hill, R. P. Ross, The sactibiotic subclass of bacteriocins: an update. *Curr. Protein Pept. Sci.* **16**, 549–558 (2015).

36. K. Takeshima, A. Chikushi, K.-K. Lee, S. Yonehara, K. Matsuzaki, Translocation of Analogues of the Antimicrobial Peptides Magainin and Buforin across Human Cell Membranes. *J. Biol. Chem.* **278**, 1310–1315 (2003).

37. M. M. Welling, A. Paulusma-Annema, H. S. Balter, E. K. J. Pauwels, P. H. Nibbering, Technetium-99m labelled antimicrobial peptides discriminate between bacterial infections and sterile inflammations. *Eur. J. Nucl. Med.* **27**, 292–301 (2000).

38. F. Ramare, *et al.*, Trypsin-dependent production of an antibacterial substance by a human Peptostreptococcus strain in gnotobiotic rats and in vitro. *Appl. Environ. Microbiol.* **59**, 2876–2883 (1993).

39. E. H. Crost, *et al.*, Ruminococcin C, a new anti-Clostridium perfringens bacteriocin produced in the gut by the commensal bacterium *Ruminococcus gnavus* E1. *Biochimie* **93**, 1487–1494 (2011).

40. A. R. Gholamiandekhordi, R. Ducatelle, M. Heyndrickx, F. Haesebrouck, F. Van Immerseel, Molecular and phenotypical characterization of *Clostridium perfringens* isolates from poultry flocks with different disease status. *Vet. Microbiol.* **113**, 143–152 (2006).

41. J. M. Stokes, A. J. Lopatkin, M. A. Lobritz, J. J. Collins, Bacterial Metabolism and Antibiotic Efficacy. *Cell Metab.* **30**, 251–259 (2019).

42. K. E. Sutyak, R. E. Wirawan, A. A. Aroutcheva, M. L. Chikindas, Isolation of the *Bacillus subtilis* antimicrobial peptide subtilosin from the dairy product-derived *Bacillus amyloliquefaciens*. *J. Appl. Microbiol.* **104**, 1067–1074 (2008).

43. M. C. Rea, *et al.*, Bioavailability of the anti-clostridial bacteriocin thuricin CD in gastrointestinal tract. *Microbiology*, **160**, 439–445 (2014).

44. F. V. Immerseel, *et al.*, *Clostridium perfringens* in poultry: an emerging threat for animal and public health. *Avian Pathol.* **33**, 537–549 (2004).

45. , Antibiotic Resistance Threats in the United States, 2019. 148 (2019).

46. W. K. Smits, D. Lyras, D. B. Lacy, M. H. Wilcox, E. J. Kuijper, *Clostridium difficile* infection. *Nat. Rev. Dis. Primer* **2**, 16020 (2016).

47. L. B. Rice, Progress and Challenges in Implementing the Research on ESKAPE Pathogens. *Infect. Control Hosp. Epidemiol.* **31**, S7–S10 (2010).

48. V. Cattoir, J.-C. Giard, Antibiotic resistance in *Enterococcus faecium* clinical isolates. *Expert Rev. Anti Infect. Ther.* **12**, 239–248 (2014).

49. K. Andries, *et al.*, A Diarylquinoline Drug Active on the ATP Synthase of *Mycobacterium tuberculosis*. *Science* **307**, 223–227 (2005).

50. S. A. Dingsdag, N. Hunter, Metronidazole: an update on metabolism, structure–cytotoxicity and resistance mechanisms. *J. Antimicrob. Chemother.* **73**, 265–279 (2018).

Figure legends

Fig. 1. Sequence and three-dimensional structure of Ruminococcin C1. (A) Sequence of RumC1 containing leader peptide (italics) and core peptide (RumC1-44), cysteine residues are underlined. **(B)** Backbone overlay of the 20 lowest target function value conformers for the DDDD stereoisomer of RumC1. **(C)** Cartoon backbone representation of the three-dimensional solution structure of RumC1 with the D stereochemistry at Ala12 (α-S), Asn16 (α-S), Arg34 (α-S) and Lys42 (α-S). Cysteine sulfur to α-carbon thioether cross-links are colored in orange and the position are indicated. **(D)** Electrostatic surface potential of RumC1, where blue indicates positive charge and red indicates negative charge. **(E)** Surface hydrophobicity of RumC1, where yellow represents hydrophobic residues and white represents hydrophilic residues.

Fig. 2. Spectroscopic characterizations of holo-RumMc1. (A) UV-vis spectrum of holo-RumMc1 in the absence (solid trace) or the presence of dithionite (dashed trace). **(B)** Mössbauer spectrum of holo-RumMc1 taken at T = 77 K with the simulation (red solid line) representing the sum of the subcomponents **1**, **2** and **3** (black lines). **1** and **2** are simulated in a ratio of 2:1 and represent two diamagnetic $[4Fe4S]^{2+}$ clusters. One $[4Fe\text{-}4S]^{2+}$ cluster is supposed to bind SAM. **3** was assigned to Fe^{3+} ions present in a $[3Fe\text{-}4S]^{1+}$ cluster in a S = 1/2 state. The respective Mössbauer parameters obtained from the simulation of the spectra at 77 K are summarized below the spectrum. **(C)** X-band CW EPR spectra of dithionite-reduced holo-RumMc1. The black line represents the experimental spectrum, while the red trace is the simulated spectrum by using three components A, B and C. **(D)** X-band CW EPR spectra of dithionite-reduced holo-RumMc1 in the presence of SAM. The black trace represents the experimental spectrum, while the red trace is the simulated spectrum by using four components A, B, C and A'. **(E)** g-values of components A, B, C and A' used to simulate the experimental EPR spectra.

Fig. 3. **Stability of RumC1. (A)** RumC1 was exposed to a range of pH for 1 hour, (**B**) to high temperatures up to 1 hour, (**C**) to human serum up to 24 hours, before measuring its MIC. (**D**) MIC of RumC1 was determined in MH medium supplemented with NaCl or $MgCl_2$. (**A to D**) All MICs were determined against *C. perfringens.* Residual antimicrobial activity was calculated based on the MIC of untreated RumC1. (**E**) Stability of RumC1 in conditions mimicking the GI tract. MIC of RumC1 against *C. perfringens* was determined after exposure to digestive enzymes. Nisin was used as a positive control of pancreatin activity. Residual antimicrobial activity was calculated based on the MIC of untreated bacteriocins. [a] Residual antimicrobial activity were measured in this study.[b] Published by Jarvis and Mahoney, 1969.

Fig. 4. Antimicrobial activity of RumC1. (A) Activity assays of RumC1 on *Bacillus cereus* grown in eukaryotic cell culture medium in the absence or the presence of a simulated intestinal

epithelium. Small and colic intestine compartments were simulated by Caco2 and T84 culture cells monolayer respectively, whereas RumC1 was added before (30 min), concomitantly and after infection (30 min) with $5x10^5$ CFU/mL *B. cereus* culture. **(B)** Activity spectrum of RumC1 against laboratory and clinical Gram-positive pathogens. Collection strains and clinical isolates are indicated. The table includes MIC of conventional antibiotics commonly used for clinical treatment and considered here as references (i.e. metronidazole, vancomycin and amoxicillin). Acquired resistance to antibiotics were determined following the EUCAST 2019 clinical breakpoint tables and are indicated by "R", whereas "i.r." refers to "intrinsic resistance", and * to the laboratory isolate references.

Fig. 5. Antibacterial mode of action of RumC1. (A, B) Cells of *C. perfringens* in early log phase were either treated with RumC1, control antibiotics, metronidazole, nisin or left untreated. Each experiment was done in independent triplicates. **(A)** After 15 min of treatment at 5xMIC, *C. perfringens* cells were incubated with radio-labelled precursors of DNA, RNA, proteins and peptidoglycan for 45 min. The synthesis of each pathway was measured by radioactivity counts. Gemifloxacin, rifampicin, tetracycline and vancomycin were used as controls antibiotics for the inhibition of DNA, RNA, proteins and peptidoglycan, respectively. Radio-labelled precursor incorporation is expressed as a percentage of maximum incorporation determined with the untreated condition. **(B)** After 15 min of treatment, the ATP present in the extracellular media (outer ATP) was measured by bioluminescence, then cells were lysed and the ATP content in the extracellular media was measured again. The inner ATP content was deduced from the difference between ATP content in the extracellular media before and after cell lysis. Cells were treated with 2.5x, 5x and 10xMIC for each condition. Relative Light Units (RLU) are expressed as percentages normalized by the value of the inner ATP content of untreated cells.

Fig. 6. **Histological analysis of human intestinal tissue treated with RumC1.** Human intestinal explants were left untreated or treated with RumC1 (100 µM) or CTAB (300 µM) for 4 h before H&E staining and microscopic observations as described in the Materials and Methods section. Images are representative of overall observed effects. Scale bar = 50 µm.

647 Figure 1

648

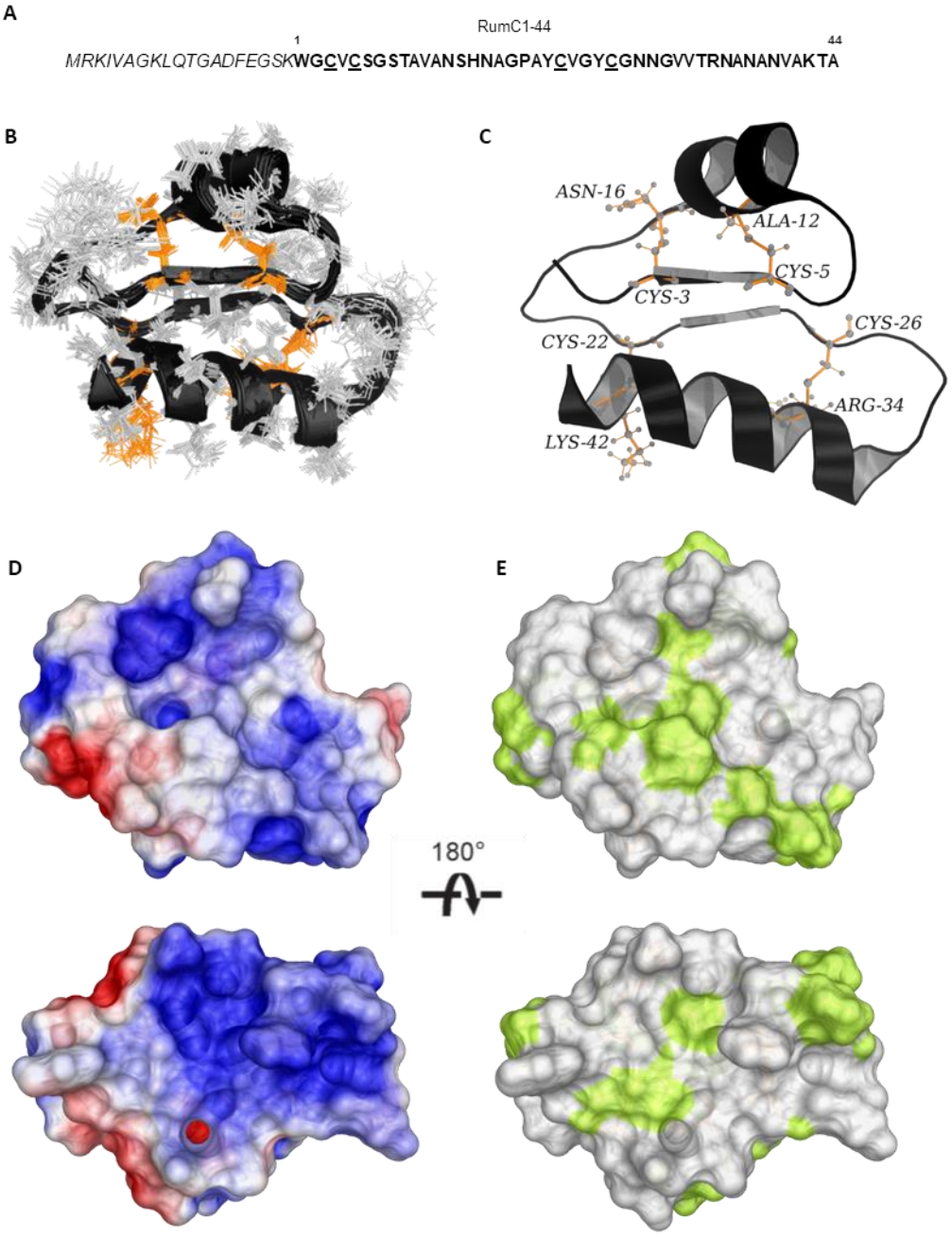

649

650

Figure 2

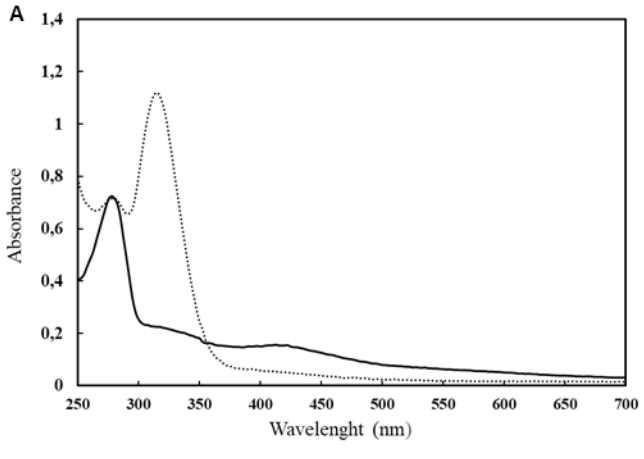

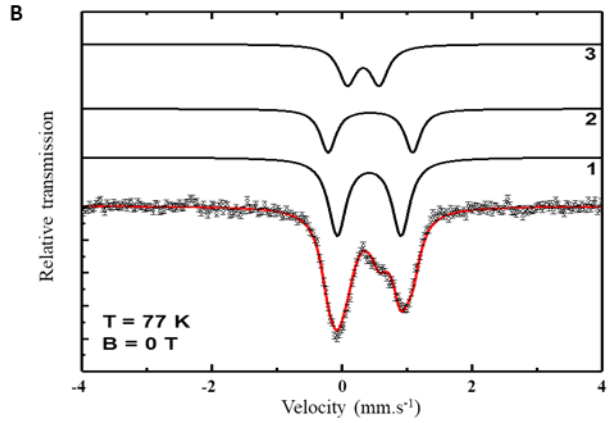

	1	2	3
δ (mms^{-1})	0.42 (± 0.01)	0.44 (± 0.01)	0.33 (± 0.02)
ΔE_q (mms^{-1})	0.98 (± 0.02)	1.30 (± 0.02)	0.49 (± 0.02)
Γ (mms^{-1})	0.33 (± 0.01)	0.29 (± 0.01)	0.33 (± 0.02)
Area (%)	50 (± 1)	25 (± 1)	25 (± 1)

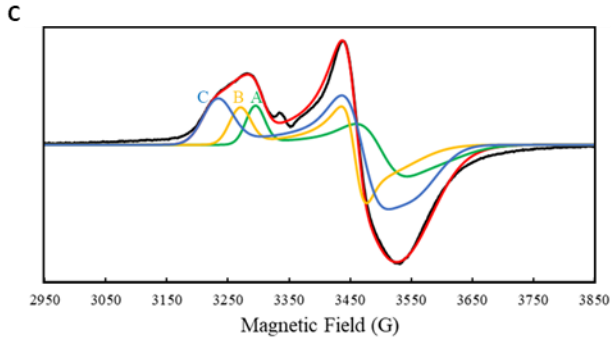

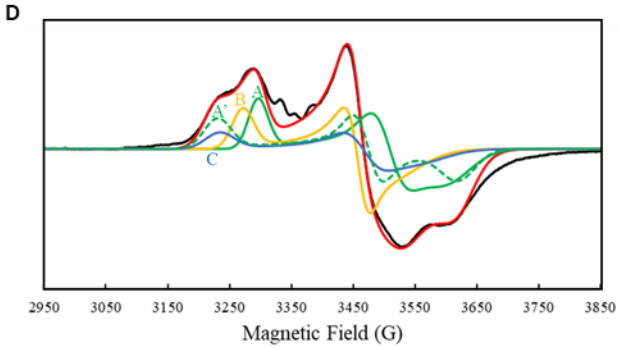

E

Proteins	SAM	A g_x g_y g_z	B g_x g_y g_z	C g_x g_y g_z	A' g_x g_y G_z
RumMc1	-	2,034(2) 1,913(2) 1,870(4)	2,050(2) 1,937(2) 1,902(4)	2,074(2) 1,932(2) 1,885(4)	
RumMc1	+	2,034(2) 1,910(2) 1,860(4)	2,049(2) 1,937(2) 1,904(4)	2,073(2) 1,932(2) 1,885(4)	2,076(2) 1,930(2) 1,852(3)

Figure 3

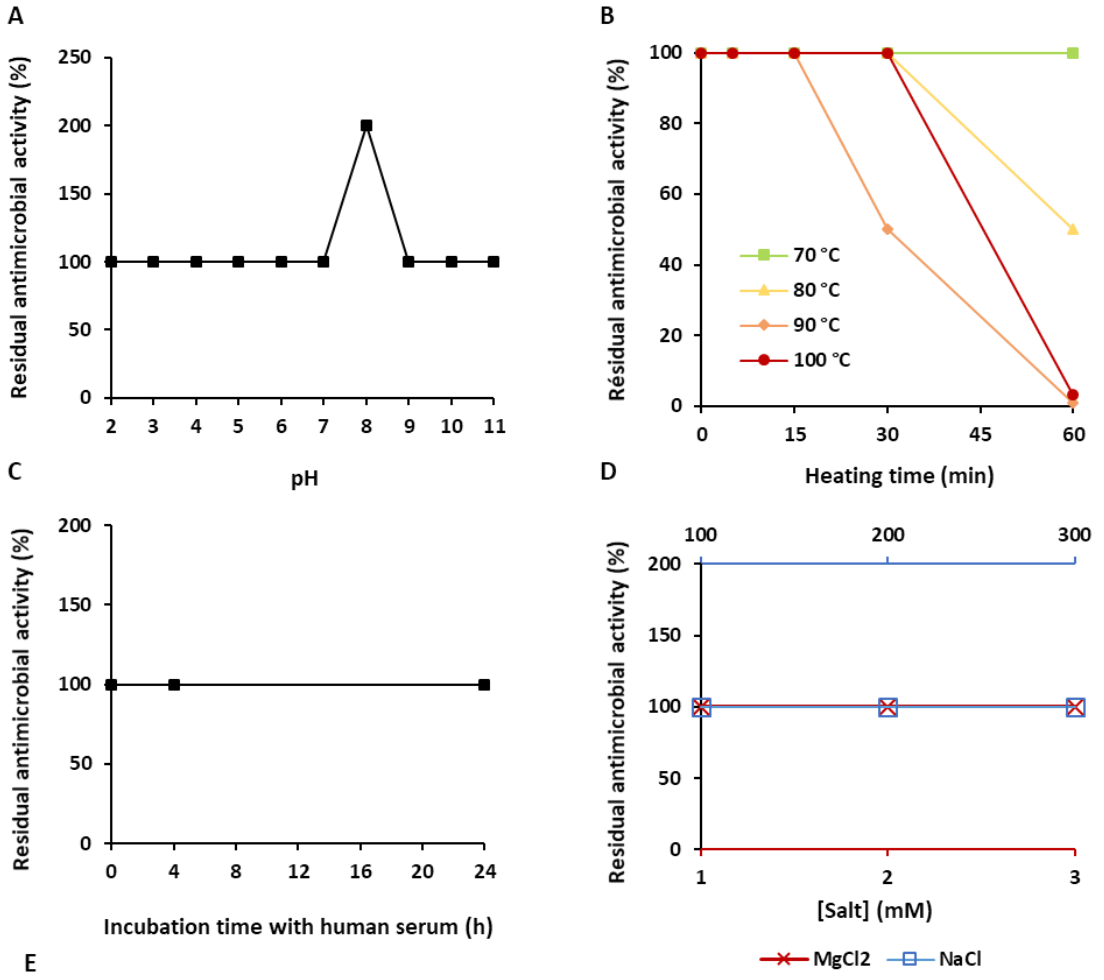

E

Simulated digestive compartment	Enzymes	pH	Temperature (°C)	Time (h)	Residual antimicrobial activity (%)	
					RumC1	Nisin
Stomac	Pepsin	2.5	37	2	100^{a}	100^{b}
Intestin	Pancreatin	6.5	37	5	100^{a}	12.5^{a}

Figure 4

A

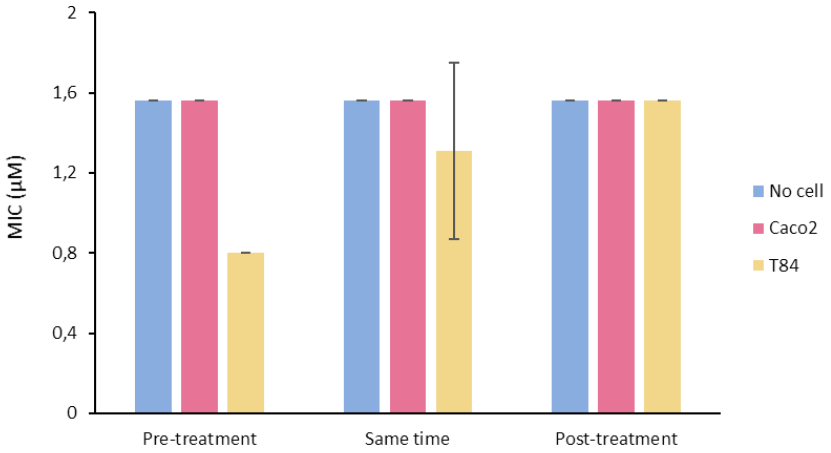

B

Organism	Source	Clinical isolate	Strain number	RumC1 MIC (µM)	Conventional antibiotics MIC (µM)		
					Metronidazole	Vancomycin	Amoxicillin
Clostridium perfringens	Laboratory	/	ATCC 13124	**0.8**	12	0.2	2.2
	Broilers	"	CP24*	**0.4**	12	0.2	2.2
	"	"	CP56*	**0.8**	12	0.2	2.2
	"	"	CP60*	**0.4**	12	0.2	2.2
	Human	Haemoculture	1*	**0.6**	23	0.4	≤ 0.3
	"	"	2*	**0.6**	23	0.4	≤ 0.3
	"	"	1600366478*	**0.6**	12	0.2	0.3
	"	"	1500022151*	**0.6**	12	0.2	0.7
	"	"	1600114439*	**0.6**	12	0.2	0.7
	"	"	1600096289*	**0.6**	12	0.2	0.7
Clostridium difficile	Laboratory	/	ATCC 700057	**0.6**	1.5	0.7	i.r.
	Human	Sacrum tissue	1600597867*	**0.3**	1.5	0.3	i.r.
Listeria monocytogenes	Human	Haemoculture	1*	**0.8**	i.r.	0.7	≤ 0.3
Bacillus cereus	Laboratory	/	CIP 5257	**1.6**	i.r.	0.7	i.r.
	Human	Haemoculture	1900276321*	**1.2**	i.r.	R	11
Streptococcus pneumoniae	Laboratory	/	ATCC 49619	**0.6**	i.r.	≤ 0.1	0.2
	Human	Haemoculture	1900304262*	**0.3**	i.r.	≤ 0.1	0.2
Enterococcus faecalis	Laboratory	/	JH2-2	**2.5**	i.r.	0.7	0.7
	Human	Haemoculture	1900302094*	**2.5**	i.r.	1.4	0.7
Enterococcus faecium	Laboratory	/	BM4147	**1.2**	i.r.	R	R
	Human	Haemoculture	1900300992*	**1.2**	i.r.	0.7	11

663 Figure 5

664

A

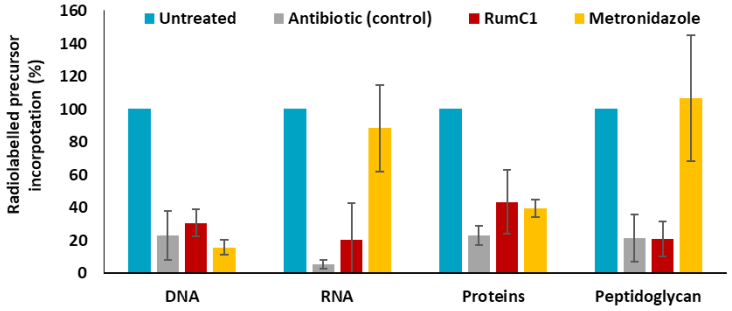

B

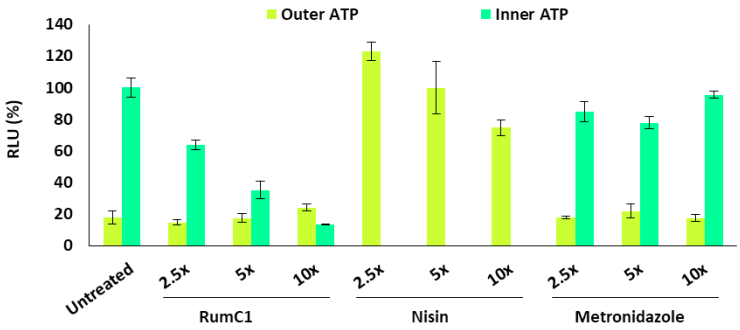

665

666

667 Figure 6

668

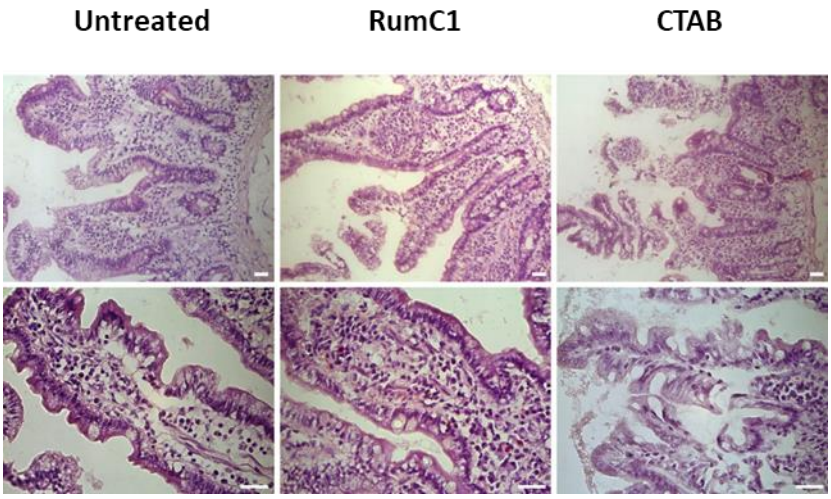

669

670

671

Supporting Information for

The unusual structure of Ruminococcin C1 antimicrobial peptide confers clinical properties

Clarisse Roblin[†], Steve Chiumento[†], Olivier Bornet*, Matthieu Nouailler, Christina S. Müller, Katy Jeannot, Christian Basset, Sylvie Kieffer-Jaquinod, Yohann Couté, Stéphane Torelli, Laurent Le Pape, Volker Schünemann, Hamza Olleik, Bruno De La Villeon, Philippe Sockeel, Eric Di Pasquale, Cendrine Nicoletti, Nicolas Vidal, Leonora Poljak, Olga Iranzo, Thierry Giardina, Michel Fons, Estelle Devillard, Patrice Polard, Marc Maresca, Josette Perrier, Mohamed Atta, Françoise Guerlesquin, Mickael Lafond*, Victor Duarte*

* Correspondence to: bornet@imm.cnrs.fr; mickael.lafond@univ-amu.fr; victor.duarte@cea.fr

† The following authors contributed equally to this work: Clarisse Roblin & Steve Chiumento

This PDF fil includes:

Figures S1 to S9

Tables S1 and S2

SI Materials and Methods

SI References

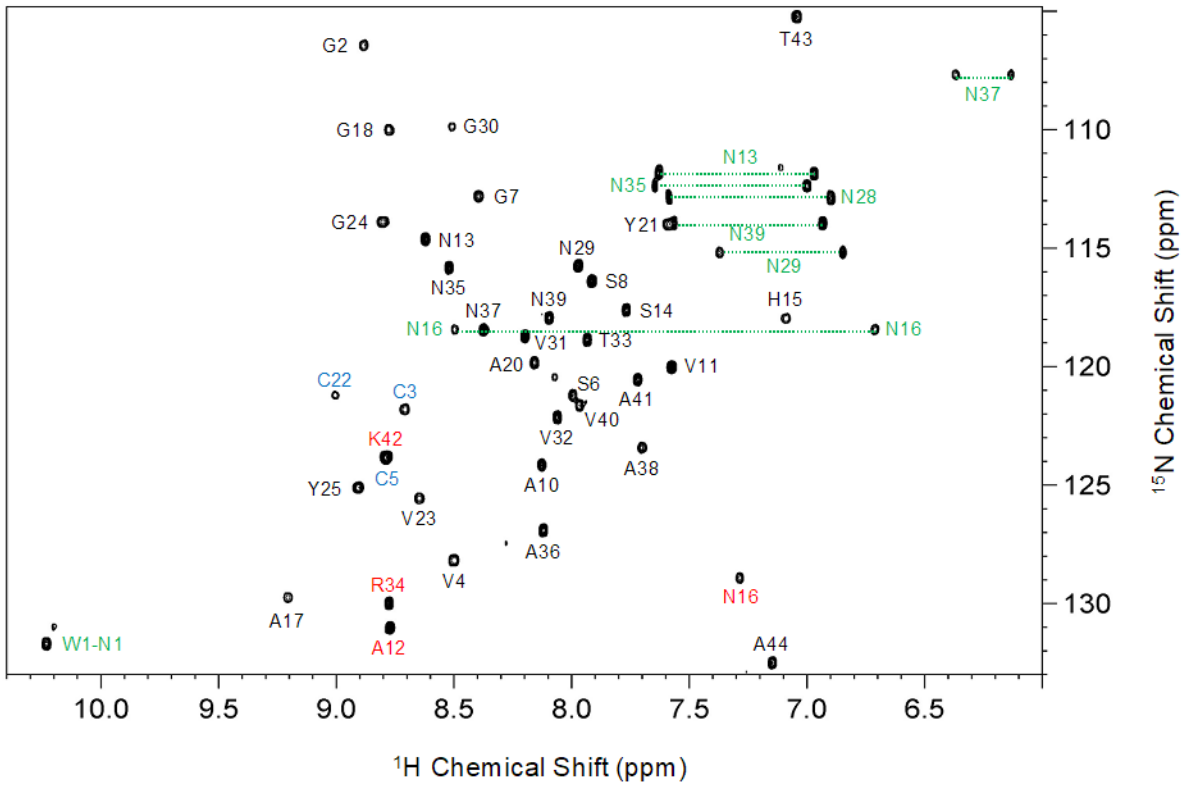

Fig. S1. Two-dimensional [^{1}H, ^{15}N] HSQC spectrum of RumC1. The number and the respective single letter code of amino acids are indicated at each assigned backbone NH cross-peak. Peaks corresponding to asparagine side chain amides are connected with a dotted horizontal line. The tryptophan indole NH group is labeled (W1-N1). Acquisition was done on a Bruker Avance III 600MHz spectrometer equipped with a cryogenically cooled 5 mm TCI probe head. Data was collected with a 0.2 mM sample concentration of ^{13}C and ^{15}N-isotopically enriched RumC1 in 10 mM phosphate buffer, pH 6.8 in 90% H_2O/ 10% D_2O at 27°C.

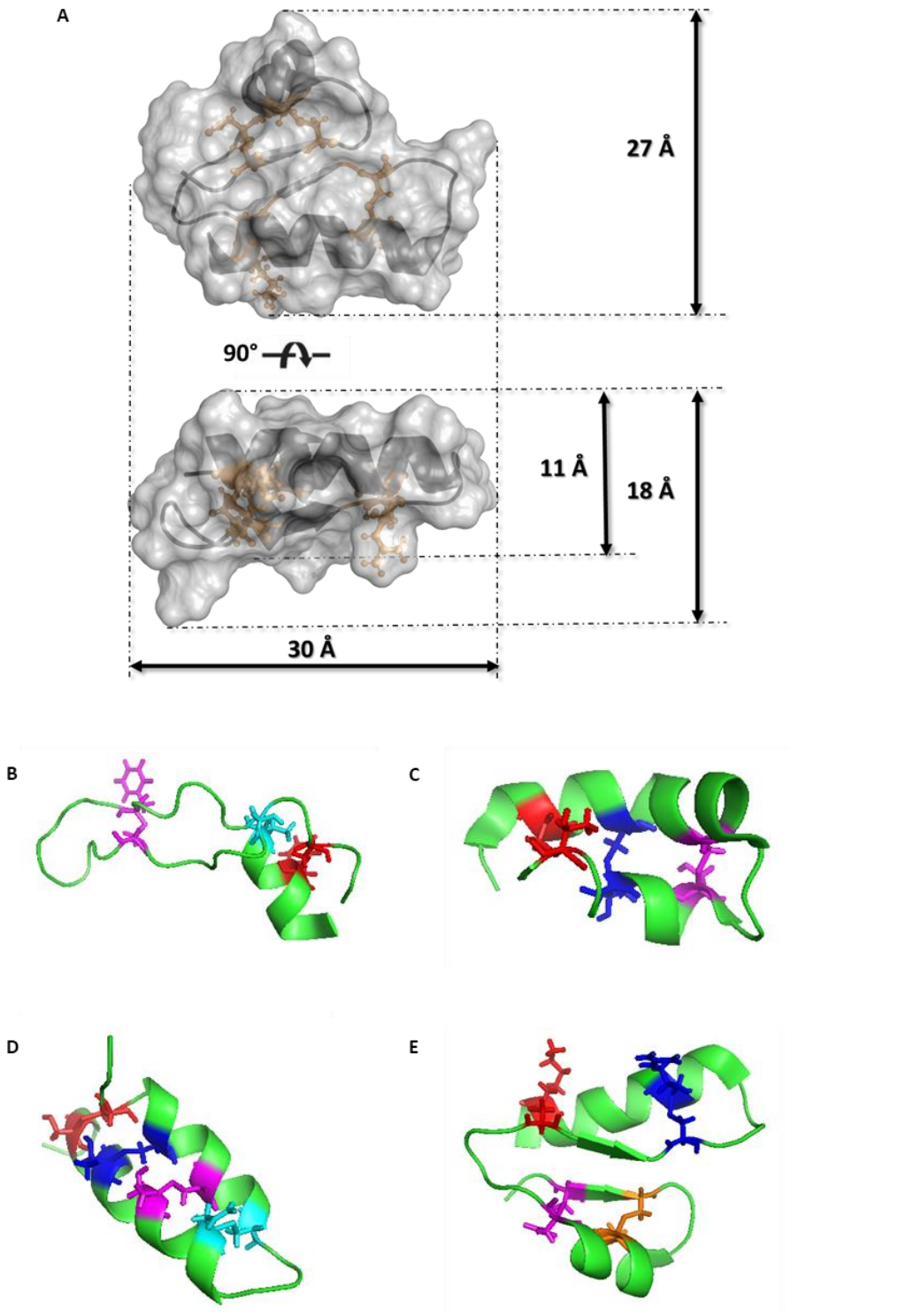

Fig. S2. Dimensions of the NMR structure of RumC1. Comparison of sactipeptides structures. (A) Dimensions of the NMR structure of the DDDD stereoisomer of RumC1. NMR Structures of: **(B)** Subtilosin A, **(C)** Thuricin CD, **(D)** Thurincin H and **(E)** RumC1. Stereoisomers at the α-carbons are LDD, LLD, DDDD and DDDD for subtilosin A, thuricin CD, thurincin H and RumC1, respectively. The Protein Data Bank codes for Subtilosin A, Thuricin CD , Thurincin H and RumC1 are 1PXQ, 2L9X, 2LBZ and 6T33, respectively.

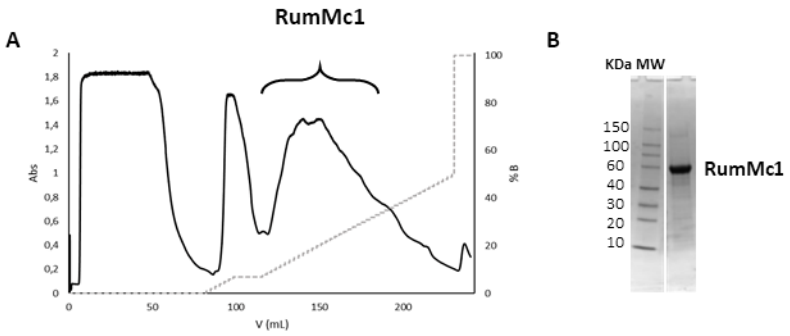

Fig. S3. Anaerobic purification of RumMc1. (A) FPLC chromatogram of overexpressed RumMc1 on a nickel-charge IMAC column. %B is the % of a 50 mM HEPES, pH 7,5, 300 mM NaCl, 500 mM imidazole buffer solution. **(B)** SDS-PAGE analysis of purified RumMc1

697

698

A

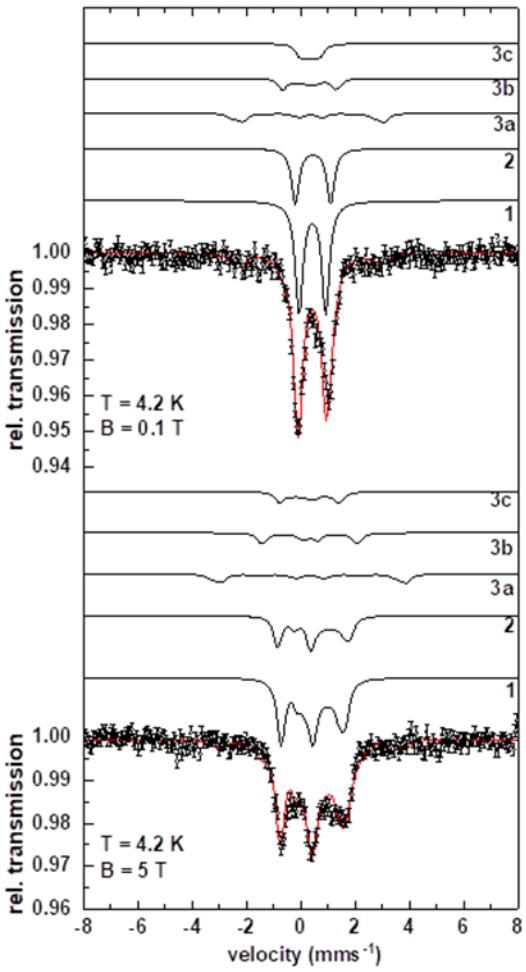

B

	1	2	3a	3b	3c
δ (mm/s)	0.42 (±0.02)	0.44 (±0.02)	0.33 (±0.03)	0.33 (±0.03)	0.33 (±0.03)
ΔE_Q (mm/s)	0.98 (±0.02)	1.30 (±0.02)	0.49 (±0.03)	0.49 (±0.03)	0.49 (±0.03)
Γ (mm/s)	0.35 (±0.02)	0.33 (±0.02)	0.33 (±0.03)	0.33 (±0.03)	0.33 (±0.03)
η	1 (-0.4)	1 (-0.4)	0 (+0.5)	0 (+0.5)	0 (+0.5)
$A_{xyz}/\mu_N g_N$ (T)	(0/0/0)	(0/0/0)	(36/28/32)[1]	(11/11/11)[1]	(2.5/2.5/2.5)[1]
Area (%)	50	25	8.33	8.33	8.33

Fig. S4. Field dependent spectra of RumMc1. (A) Mössbauer spectra of RumMc1 with the simulation (red solid line) representing the sum of the subcomponents **1**, **2** and **3** (black lines). Component **1** and **2** are simulated in a ratio of 2:1 and represent two diamagnetic $[4Fe4S]^{2+}$ clusters. Component **3** is divided into three subcomponents **3a**, **3b** and **3c** that represent three Fe^{3+} high spin ions antiferromagnetically coupled to a total spin of S = 1/2 as present in a $[3Fe4S]^{1+}$ cluster. **(B)** Mössbauer parameters obtained from the simulation of the field dependent spectra of RumMc1. [1] Values for $A_{xyz}/\mu_N g_N$ were taken from B. H. Huynh *et al.* (1).

Fig. S5. Alignment of selected radical-SAM enzymes with RumMc1. Alignment of anSME (anaerobic Sulfatase Maturating Enzyme), AlbA, and RumMc1. Conserved residues are marked "*" and cysteine residues are highlighted in green.

A

	RumC1	RumC1-44	RumC1-44-LS
% maturation	90%	< 1%	< 10%

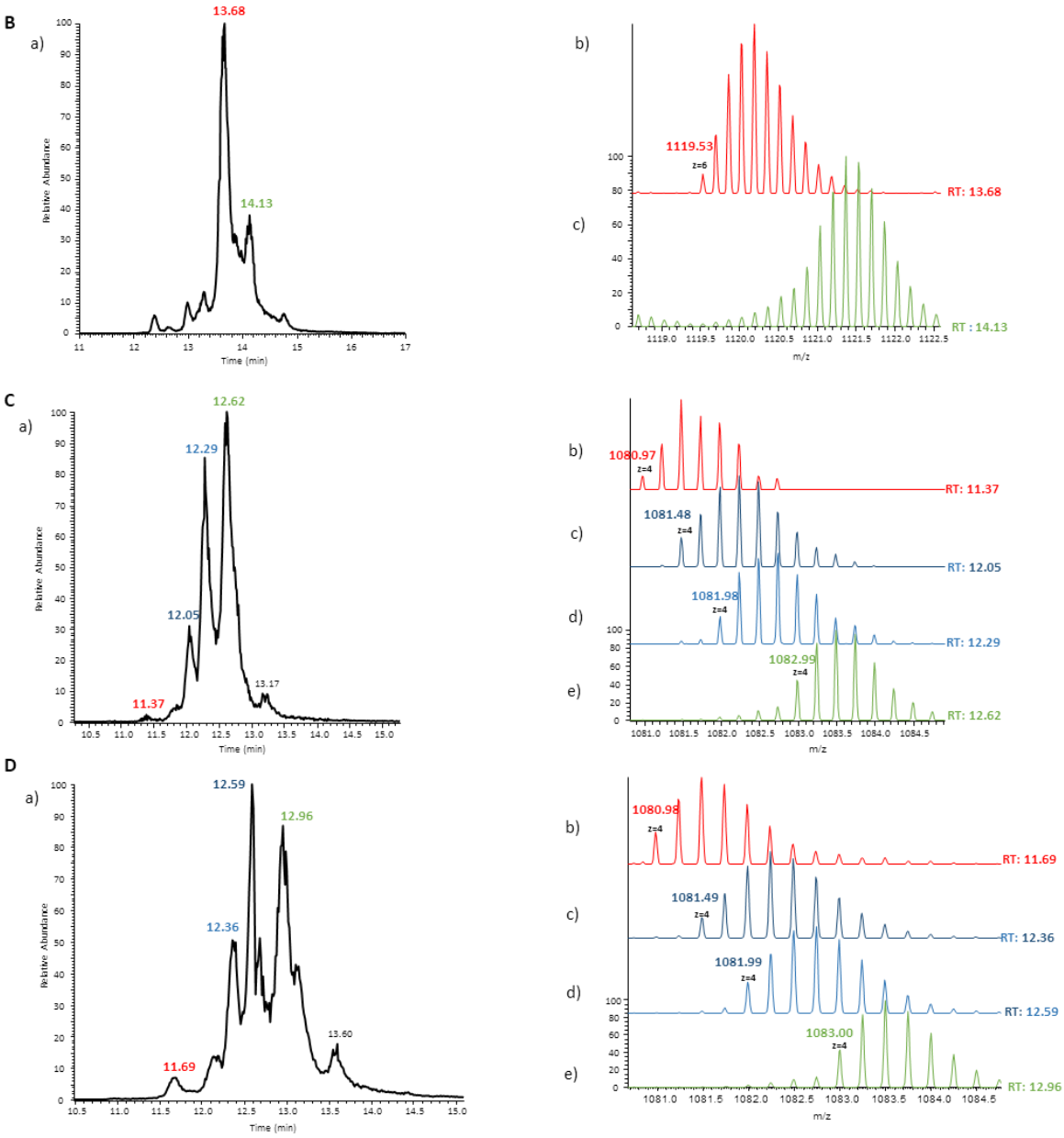

Fig. S6. LC-MS analyses of leader peptide-dependent maturation of RumC1. (A) Percentage of the full maturation for the different constructions. **(B)** Maturation of RumC1: (a) LC-MS trace of *in vitro* matured RumC1. Zoom-in spectra at RT = 13.68 (b) and RT = 14.13 (c) for m/z corresponding to RumC1. (b) A major ion $[M+6H]^{6+}$ = 1119.5 Da corresponds to the fully maturated form containing 4 thioether bonds. (c) A mixture of unmaturated forms containing no, one or two disulfide bonds are observed. **(C)** Maturation of RumC1-44: (a) LC-MS trace of *in vitro* matured RumC1-44. Zoom-in spectra at RT = 11.37 (b), RT = 12.05 (c), RT = 12.29 (d), and RT = 12.62 (e) for m/z corresponding to RumC1-44. (b) A major ion $[M+4H]^{4+}$ = 1081 Da corresponds to the fully maturated form containing 4 thioether bonds. (c) A major ion $[M+4H]^{4+}$ = 1081.5 Da corresponds to a species containing 3 thioether bridges. (d) A major ion $[M+4H]^{4+}$ = 1082 Da corresponds to a species with 2 thioether bridges. (e) A major ion $[M+4H]^{4+}$ = 1083 Da corresponds to the non maturated form of RumC1-44. **(D)** Maturation of RumC1-44-LS: (a) LC-MS trace of *in vitro* matured RumC1-44-LS. Zoom-in spectra at RT = 11.69 (b), RT = 12.36 (c), RT = 12.59 (d), and RT = 12.96 (e) for m/z corresponding to RumC1-44-LS. (b) A major ion $[M+4H]^{4+}$ = 1081 Da corresponds to the fully maturated form containing 4 thioether bonds. (c) A major ion $[M+4H]^{4+}$ = 1081.5 Da corresponds to a species containing 3 thioether bridges. (d) A major ion $[M+4H]^{4+}$ = 1082 Da corresponds to a species with 2 thioether bridges. (e) A major ion $[M+4H]^{4+}$ = 1083 Da corresponds to the non maturated form of RumC1-44-LS.

709

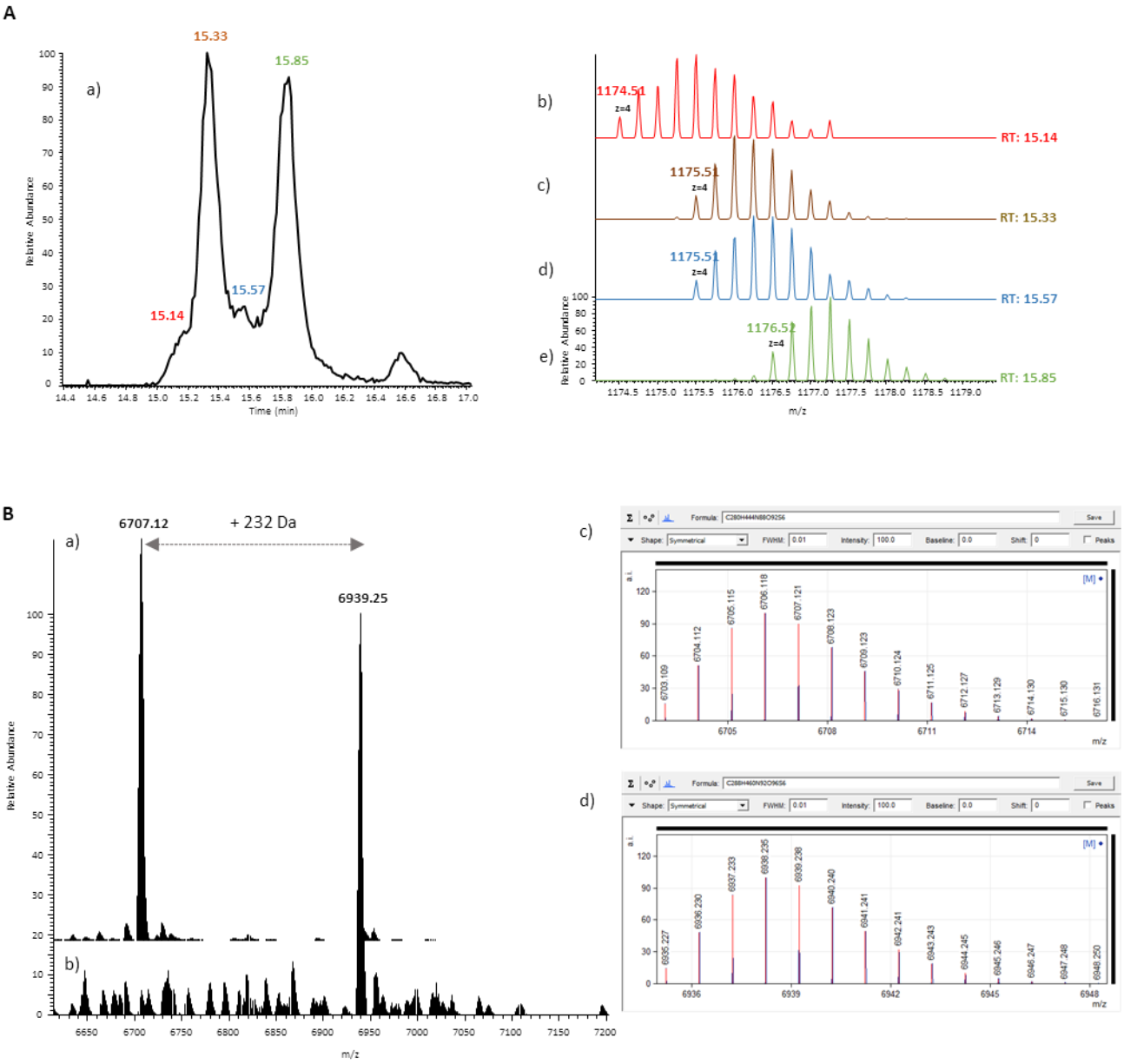

Fig. S7. Analysis of *in vivo* maturation of RumC1-44 and RumC1-Ala18/Ala19 variant. (A) LC-MS analysis of *in vivo* maturated RumC1-44. (a) LC-MS trace of *in vivo* matured RumC1-44. Zoom-in spectra at RT = 15.14 (b), RT = 15.33 (c), RT = 15.57 (d) and RT = 15.85 (e) for m/z corresponding to RumC1-44. (b) A major ion $[M+4H]^{4+}$ = 1174.5 Da corresponds to the fully maturated form containing 4 thioether bonds. (c) and (d) A major ion $[M+4H]^{4+}$ = 1175.5 Da corresponds to species with respectively 2 disulfide bridges and 2 thioether bridges, according to their corresponding MS/MS spectra. (e) A major ion $[M+4H]^{4+}$ = 1176.5 Da corresponds to the non maturated form of RumC1-44. **(B)** MS Analysis of *in vivo* maturated RumC1-Ala18/Ala19. (a) The deconvoluted mass obtained for the main species is 6707.1 and corresponds to a species containing 2 disulfide bridges. (b) After DTT reduction and iodoacetamide alkylation, the mass is shifted to 6939.2 corresponding to RumC1-Ala18/Ala19 alkylated 4 times (mass increased by 232 Da corresponding to 4 alkylations and 2 disulfide bridge reductions). (c) and (d) Simulated MS profiles of RumC1-Ala18/Ala19 with disulfide bonds and fully alkylated cysteines, respectively.

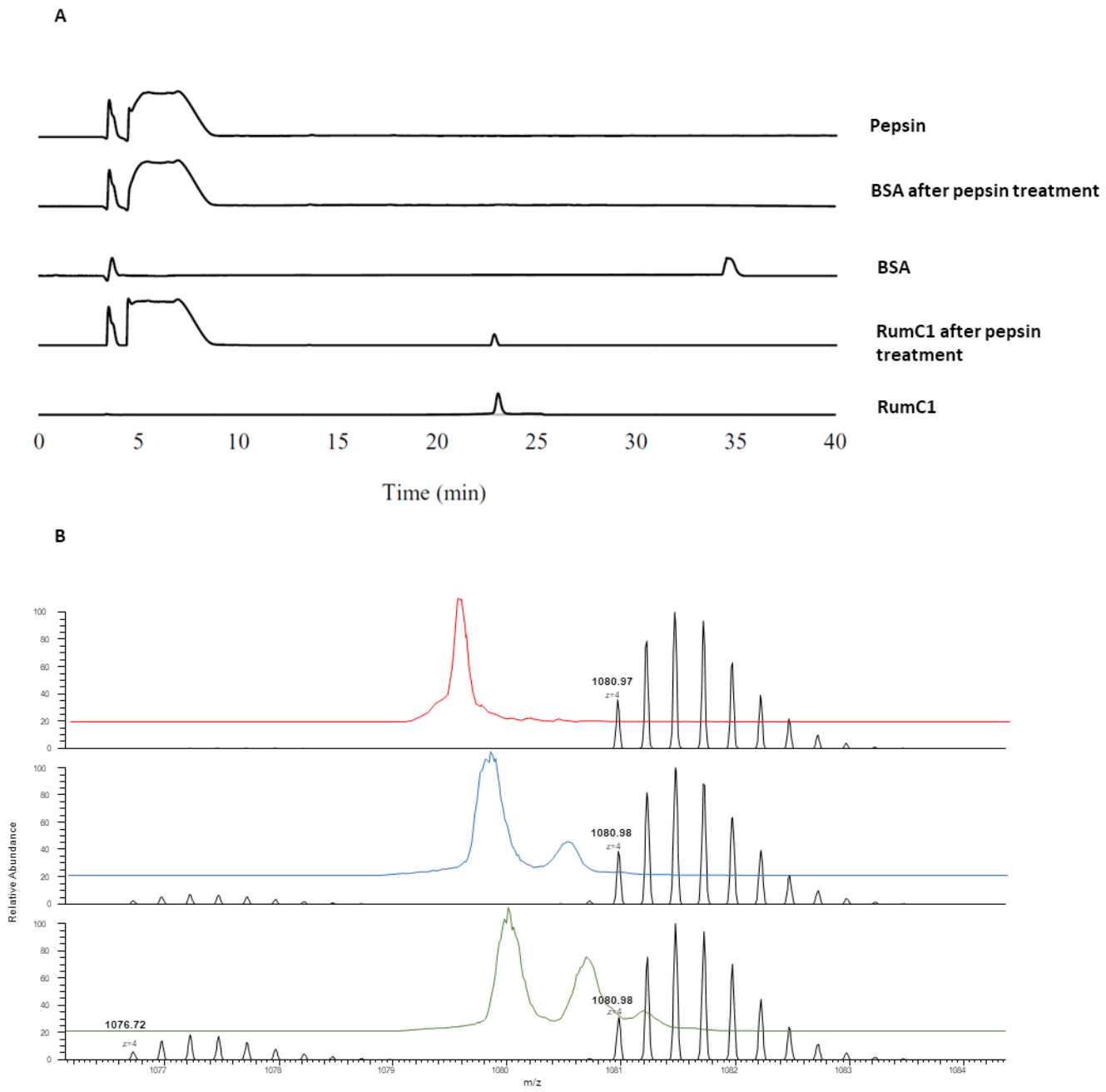

Fig. S8. Chromatographic and spectroscopic analyses to evaluate RumC1 integrity. (A) Chromatogram of RP-C18-HPLC of RumC1, or BSA used as control, treated with pepsin and in conditions simulating the stomach (pH 2,5 37°C 2h). **(B)** LC-MS profiles and MS spectra of RumC1 (top, red) submitted to pepsin (middle, blue) or pancreatic conditions (bottom, green). No change on RumC1 was observed after digestion except the presence of a light amino loss species due to heating (-NH3).

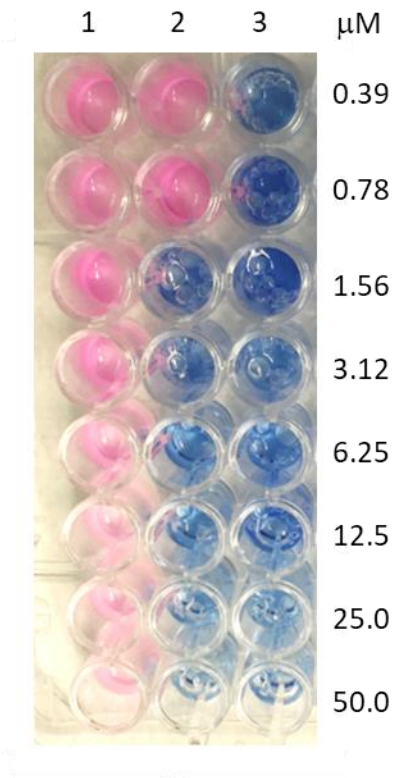

Fig. S9. **Evaluation of RumC1 activity on simulated intestinal epithelium infected by *Bacillus cereus*.** After 24h of incubation, suspension of *B. cereus* grown on Caco-2 and T84 cells were transferred to new 96 well plates free of eukaryotic cells. Resazurin was added to determine the viability of the bacterial cells. Briefly, resazurin is a blue dye that is reduced in pink resorufin in the presence of metabolically active cells. An example of untreated *B. cereus* grown on Caco-2 cells is shown in column 1, whereas the column 2 corresponds to *B. cereus* grown on Caco-2 cells with increasing concentrations of RumC1 and column 3 represents uninfected and untreated Caco-2 cells.

715

716

Table S1. Comparison of statistics generated by the 16 stereoisomers of RumC1. Assigned NOEs represent total number of off-diagonal NOE assignments used by CYANA to perform the structure calculation.

Table entry	Isomers	Thioether bond violations	Assigned NOEs	RMSD (Angstroms)	CYANA average target function value
1	LLLL	3	374	2.5 ± 0.4	0.7
2	LLLD	3	385	1.9 ± 0.8	2.0
3	LLDL	2	400	1.3 ± 0.5	1.3
4	LLDD	2	371	2.7 ± 0.4	3.8
5	LDLL	3	399	1.4 ± 0.5	1.2
6	LDLD	4	404	1.2 ± 0.3	1.5
7	LDDL	3	398	1.1 ± 0.3	0.7
8	LDDD	1	399	1.4 ± 0.2	0.6
9	DLLL	3	405	1.6 ± 0.3	1.1
10	DLLD	4	430	1.5 ± 0.2	0.7
11	DLDL	8	406	2.3 ± 0.4	2.9
12	DLDD	6	377	2.5 ± 0.6	5.3
13	DDLL	3	405	1.5 ± 0.5	1.3
14	DDLD	2	404	1.3 ± 0.2	0.7
15	DDDL	1	394	1.2 ± 0.2	0.3
16	DDDD	0	417	0.9 ± 0.2	0.1

Table S2. Structure calculation statistics for the DDDD stereoisomer of RumC1. Statistics for structure calculation refers to all the twenty structures.

Final NMR restraints in the DDDD structure calculation		
Short-range ($\|i-j\| = 1$)	317	
Medium-range ($1<\|i-j\| < 5$)	99	
Long-range ($\|i-j\| \geq 5$)	80	
Total nOe distance restraints	496	
Hydrogen bonds	50	
Thioether Bridge distance restraints	8	
Dihedral angle restraints	46	
Total restraints	600	13.6 restraints/residu
Residual violations		
CYANA target function	0.36 +/- 1.08	
NOE upper distance constrain violation		
Number > 0.1 Å in at least 1 structure	7	
Dihedral angle constrain violations		
Number > 0.1°	0	
Van der Waals violations		
Number > 0.1 Å	0	
Average structural RMSD to the mean coordinates (Å)		
All backbone atoms	0.81 +/- 0.50	
All heavy atoms	1.19 +/- 0.54	
Ramachandran statistics, % of all residues		
Most favored regions	84.1	
Additional allowed regions	15.4	
Generously allowed regions	0.4	
Disallowed regions	0	

SI Materials and Methods

Heterologous expression and purification of (^{13}C, ^{15}N)-labelled mature RumC1. A synthetic plasmid containing the *E. coli* codon-optimized gene of *R. gnavus* E1 encoding RumMc1 (pET-15b-*rumMc1*, ampicillin-resistant) was obtained from Genscript. Plasmids pET-15b-*rumMc1*, pETM-40-*rumC1* and psuf (chloramphenicol-resistant) containing *sufABCDSE* genes were used to transform competent *E. coli* BL21 (DE3) cells for expression. The resulting strain was grown in 3 L of M9 medium containing kan (50 μg/mL), amp (100 μg/mL), chl (34 μg/mL), vitamin B1 (0.5 μg/mL), $MgSO_4$ (1 mM), $FeCl_3$ (50 μM) and glucose (4 mg/mL) at 37 °C. At an optical density (OD_{600}) of 0.25, cells were harvested by centrifugation (4,000 rpm for 20 min at 4°C). The cells were resuspended in 1 L of labeled minimal medium (Na_2HPO_4 6 g/L, KH_2PO_4 3 g/L, $^{15}NH_4Cl$ 1 g/L) containing kan (50 μg/mL), amp (100 μg/mL), chl (34 μg/mL), vitamin B1 (0.5 μg/mL), $MgSO_4$ (1 mM), $FeCl_3$ (50 μM) and labeled glucose-^{13}C (4 mg/mL). The culture was grown at 25°C to an optical density (OD_{600}) of 0.8. $FeCl_3$ (100 μM) and L-cysteine (300 μM) were then added and the culture was induced with 1 mM IPTG. The cells were grown for 15h under stirring and then were harvested by centrifugation (4,000 rpm for 20 min at 4°C). Labelled MBP-RumC1 was purified as described for the MBP-RumC1 (2). (^{13}C, ^{15}N)-labelled mature RumC1 was obtained after cleavage of the MBP tag by using TEV and purified as previously reported (2). Leader peptide cleavage was performed with trypsin as described by Chiumento *et al.*, (2). Briefly, labelled RumC1was treated with TPCK (N-tosyl-L-phenylalanine chloromethyl ketone)–treated trypsin (Sigma-Aldrich) for 1 hour at 37°C at a molar ratio of 200:1 (RumC1:trypsin). Then RumC1 was purified using RP-C18-HPLC with the following gradient: 10 min at 22% followed by 12 min from 22 to 38% of 90% ACN and 0.1% TFA, on a preparative column (250 mm by 21.2 mm; Phenomenex, Jupiter, 15 μm, 300 Å).

NMR spectroscopy of RumC1. The NMR sample used for sequential assignment of ^{13}C-^{15}N-labeled RumC1 was approximately 0.2 mM in 10 mM phosphate buffer, 90% H_2O/10% D_2O at pH 6.8. All NMR data were collected at 27°C using a Bruker Avance III 600 MHz NMR spectrometer equipped with a TCI 5 mm cryoprobe. The following datasets were performed; 2D: [^{15}N,^{1}H] HSQC and [^{13}C,^{1}H] HSQC; 3D: [^{1}H,^{15}N,^{13}C] HNCACB, CBCA(CO)NH, HNCA, HN(CO)CA, HNCO, HN(CA)CO, ^{13}C-TOCSY-HSQC (spin lock of 80 ms) and (H)CCH-TOCSY. Backbone resonances were assigned from triple resonance spectra and were extended to give side chain assignments using (H)CCH-TOCSY and ^{13}C-TOCSY-HSQC. ^{1}H assignments for aromatic side chains and asparagines side chain amides were made using 2D [^{1}H, ^{1}H] TOCSY and NOESY (mixing time of

150 ms) spectra. Spectra were processed with Topspin 3.5 and analyzed with CcpNmr Analysis software (3). All of the peak lists and the complete ^{1}H, ^{13}C and ^{15}N backbone and side chain chemical shift assignments have been deposited into the Biological Magnetic Resonance Databank (http://www.bmrb.wisc.edu) under ascension code 50027.

Structure Calculations. For the structure calculations, a 2D [^{1}H, ^{1}H] NOESY was acquired with a mixing time of 150 ms, using a 2 mM unlabeled RumC1 sample in 10 mM phosphate buffer, 90% H_2O/ 10% D_2O, pH 6.8 at 27°C, performed on the Bruker Avance III 600 MHz spectrometer. The structures of the 16 stereoisomers were calculated with CYANA 2.1 (4), using NOE restraints measured from the 2D [^{1}H, ^{1}H] NOESY, 3D [^{1}H, ^{15}N, ^{1}H] NOESY, 3D [^{1}H, ^{13}C, ^{1}H] NOESY experiments and angle restraints obtained from the TALOS+ server (5). The NOEs were calibrated within CYANA according to their intensities. The same nOe peaks list and angle restraints were used for the structure calculations of each stereoisomer, following the same procedure as previously described by John Vederas and co-workers (6–8). Twenty lowest target function value conformations were generated for each of the 16 stereoisomers. Coordinates of the twenty conformations of DDDD stereoisomer of RumC1 have been deposited into the Protein Data Bank under ascension code 6T33.

Expression of RumMc1. We obtained a commercially supplied codon-optimized synthetic plasmid of *Ruminococcus gnavus* RumMc1 (pET-28a–*rumMc1*, kanamycin-resistant) from Genscript. Vectors pET-28a-*rumMc1* and pDB1282 (ampicillin-resistant), which carries the *isc* operon required for proper assembly of the Fe-S clusters in RumMc1, were subsequently co-transformed into chemically-competent BL21 (DE3) *E. coli* cells. A 500 mL sterile culture erlenmeyer containing 100 mL Luria Bertani medium (LB) supplemented with kan (50 μg/mL), amp (100 μg/mL) was inoculated with a single colony of BL21 (DE3) cells carrying pET-28a-*rumMc1* and pDB1282. The 100 mL culture was grown overnight at 37 °C, 200 rpm and used to inoculate 10 liters M9 minimal medium on a fermenter. The minimal medium was prepared by supplementing M9 Minimal Salts (Sigma) with a final concentration of 20 mM glucose, 2 mM MgSO4, 50 μg/mL kan, 100 μg/mL amp) and 50 μM $FeCl_3$. The fermenter culture was grown at 37 °C, 200 rpm to an OD_{600} nm ~ 0.3-04 and then supplemented with a final concentration of 50 μM $FeCl_3$, 300 μM L-Cys, and 13.3 mM L-arabinose. At an (OD_{600}) of 1.2, the culture was cooled at 24°C, supplemented with a final concentration of 1 mM IPTG and grown for 15h under stirring. The cells were harvested by centrifugation (4,000 rpm for 20 min at 4°C).

Purification of RumMc1. The purification protocol was carried out under strictly anaerobic conditions. The cell pellet was suspended in 40 mL of buffer A (50 mM HEPES, pH 7.5, 300 mM NaCl), sonicated and lysate clarified by centrifugation at 40,000 rpm at 4 °C for 40 min. The supernatant was collected and passed over nickel-charge IMAC column (HisTrap^{TM} HP 5mL GE Healthcare). Columns were washed with 4 volumes of buffer A. RumMc1 was eluted from nickel-charge IMAC columns with a gradient of 0-50% of buffer B (50 mM HEPES, pH 7.5, 300 mM NaCl, 500 mM imidazole). Fractions containing RumMc1were pooled and concentrated in a 30,000 MWCO filter in an Amicon® Ultra centrifugal filter devices. To eliminate imidazole and salts, sample was passed on NAP^{TM} Column, NAP-25 equilibrated in buffer C (HEPES 50mM, NaCl 100 mM pH 7.5). Anaerobic UV-visible spectra were recorded on an Uvikon XL100 spectrophotometer (Bio-Tek instruments) connected by optical fibers to the cuvette holder in the anaerobic chamber. The protein concentration was estimated by UV-visible spectroscopy by using an extinction coefficient at 280 nm of 73266 $M^{-1}.cm^{-1}$. Iron content of RumMc1 samples were measured according to the Fish method (ref). The calibration curve was obtained by measuring iron standards with iron content form 2 to 30 nmol.

Site directed mutagenesis of *rumC1* and heterologous expression of RumC1 variant. Site directed mutagenesis of the *MBP-rumC1* construct was performed to produce the Ala18/Ala19 variant of RumC1. Mutagenesis was done by following the instructions from the Q5 Site-Directed Mutagenesis Kit (New England BioLabs®). The NEBaseChanger tool was used to generate the 2 primer sequences (5'-CCATAACGCGGCTGCGGCGTACTGCG, 5'-CTGTTCGCAACCGCGGTG) and annealing temperatures. Template plasmids were digested using DpnI and were transformed into competent Top10 cells. The mutant plasmids were recovered from cells by using the Wizard® Plus SV Minipreps DNA Purification System (Promega).
Production and purification of RumC1-Ala18/Ala19 variant were performed as previously described for RumC1 (2).

Leader-peptide chemical synthesis

Chemicals

The N-fluorenylmethoxycarbonyl (Fmoc)-protected amino acids, rink amide MBHA resin (100 - 200 mesh) and 2-(1H-Benzotriazole-1-yl)-1,1,3,3-tetramethyluronium hexafluorophosphate (HBTU) were obtained from Novabiochem; N,N-diisopropylethylamine (DIEA), trifluoroacetic acid (TFA), anisole, thioanisole, 1,2-ethandithiol, acetic anhydride, piperidine and triethylamine (TEA) were from Sigma-Aldrich. All the other chemicals and solvents (N,N-dimethylformamide

(DMF), diethyl ether, dichloromethane (DCM), acetonitrile (ACN) and N-methyl-2-pyrrolidone (NMP) were from different commercial sources (highest available grade) and used without further purification.

Peptide synthesis

The leader sequence of RumC1 peptide (H_2N-MRKIVAGKLQTGADFEGSK-NH_2) was prepared by solid phase peptide synthesis in an Initiator$^+$ Alstra automated microwave assisted synthesizer (Biotage). The peptide was assembled on a rink amide MBHA resin (0.25 mmol scale, 0.59 mmol/g) using standard Fmoc methodologies (9). Namely, the amino acids (4 equiv) were coupled using HBTU (3.9 equiv) as coupling agent, DIEA as base (8 equiv) and DMF as solvent. The removal of the Fmoc protecting groups was always done by treating the resin with 20% piperidine in DMF solution. After assembling, the peptide was manually deprotected and cleaved from the resin by treatment with the mixture TFA/thioanisole/anisole/1,2-ethandithiol (%v/v = 90:5:3:2) for 2 h at room temperature and under nitrogen. The resin was filtered out and rinsed with TFA. The filtrate and rinses were combined, reduced under a nitrogen stream and slowly added to cold diethyl ether with magnetic stirring to precipitate the crude peptide. The suspension was transferred to a centrifuge to recover the peptide which was washed with cold diethyl ether and centrifuged again. This step was repeated several times and finally the crude peptide was dissolved in the minimum amount of water and lyophilized. The crude peptide was purified by preparative reversed-phase HPLC in a Phenomenex Jupiter column (250 mm × 21.20 mm, 15 μm, 300 Å) using solvent A (99.9% water/0.1 % TFA) and solvent B (90% ACN/9.9% water/0.1 % TFA). The leader sequence of RumC1 peptide was eluted with a linear gradient from 15% to 35% B in 30 min at a flow rate of 10 mL/min (R_t = 14 min). Its purity was checked by analytical reversed-phase HPLC (Phenomenex Jupiter column, 250 mm × 4.6 mm, 15 μm, 300 Å) and it was greater than 95%. The peptide was characterized by Electrospray Ionization-Mass spectrometry (ESI-MS) in positive mode using a Waters Synapt G2 HDMS (Manchester, UK) equipped with an ESI source employing the following parameters: ESI capillary voltage: +2.8 kV; extraction cone voltage: +20 V; desolvation gas (N2) flow: 100 $L.h^{-1}$; source temperature: 35 °C. Sample solutions were introduced in the ionization source at a 10 $\mu L.min^{-1}$ flow rate using a syringe pump.

***In Vitro* Enzyme Assay.** The *in vitro* enzymatic assays were performed in 100 µl of 100 mM HEPES, pH 7.5, in the presence of 100 µM of the desired peptide substrate, 25 µM of RumMc1 protein, 0.25 mM SAM and 1 mM dithionite. The assays were carried out at 37 °C during 3h under anaerobic conditions. The reactions were stopped by air exposure and were flash frozen in liquid nitrogen.

EPR and Mössbauer spectroscopies. EPR and Mössbauer samples (400 µM) were prepared and flash frozen under anaerobic conditions. When needed, cluster reduction was achieved in 1 hour by addition of 10 mM dithionite. Samples in the presence of SAM were prepared with 3 mM SAM. EPR spectra were recorded on a Bruker EMX spectrometer operating at X-band frequency equipped with an Oxford instrument ESR 900 flow cryostat. Spectra were recorded with a microwave frequency 9.65 GHz under saturated (10K, 39dB, modulation amplitude 10 G) and non-saturated (6K, 13dB, modulation amplitude 10 G) conditions for the g = 2 region. Simulations were performed using Easy Spin toolbox for matLAB. Mössbauer spectra were recorded in transmission mode with a conventional Mössbauer spectrometer which was operated in the constant acceleration mode in conjunction with a multi-channel analyzer in the time-scale mode (WissEl GmbH). The spectrometer was calibrated against α-iron at room temperature. Experiments at 77 K were conducted using a flow cryostat (Optistat^{DN}, Oxford Instruments). Field-dependent Mössbauer spectra were obtained with a helium closed-cycle cryostat (CRYO Industries of America, Inc.) equipped with a superconducting magnet (10). The magnetic field was aligned parallel to the γ-ray beam. The spectral data were transferred from the multi-channel analyzer to a PC for further analysis employing the public domain program Vinda (11) running on an Excel 2003® platform. Analysis of the spectra was performed by least-squares fits using Lorentzian line shapes with the linewidth Γ. Field-dependent spectra were simulated by means of the spin Hamilton formalism (12).

Nano-LC−MS/MS Analyses. RumC1 samples were generally injected at a concentration of 0.1 µM. Samples were diluted in 5% (v/v) acetonitrile and 0.1% (v/v) trifluoroacetic acid and analysed by online nano-LC−MS/MS (NCS HPLC, Dionex, and Qexactive HF, Thermo Fisher Scientific). Peptides were sampled on a 300 µm × 5 mm PepMap C18 precolumn and separated on a 75 µm × 250 mm C18 column (PepMap, Dionex). The nano-LC method consisted of a 40 min gradient at a flow rate of 300 nL/min, and MS and MS/MS data were acquired using Xcalibur (Thermo Fisher Scientific). In order to improve the quality of the MS/MS spectra we performed parallel reaction monitoring (PRM) experiments to characterize RumC1 species. According to our previous characterization of RumC1 (Chiumento et al., 2019), we decided to focus these analyses on the highest m/z ions for the long (with leader peptide) and short (without leader peptide) peptides (respectively m/z = 1120 (6^+) and m/z = 1083 (4^+)). The m/z window was open at 4 units in order to consider modified species. The collision energy was set to 27.

The MS interpretations were done on the basis of previously annotated spectra and specific fragmentation pattern of thioether bridges using HCD (2). Mascot (version 2.6) was also used for the confirmation of the modifications, as previously described (2).

Stability assays. Stability of RumC1 was evaluated after incubation varying pH, temperatures, and in human serum. RumC1 was incubated in phosphate-buffered saline (PBS) at pH range from 2 to 11 at a volume ratio of 1:1 for 1 hour at room temperature. In a second assay RumC1 was incubated at temperatures of 70, 80, 90 and 100 °C for 5, 15, 30 or 60 minutes before being cooled on ice. Finally, RumC1 was incubated in human serum (Sigma Aldrich) at a volume ratio of 1:1 for 4 or 24 hours at 37°C with stirring (180 rpm). After each of this treatment, Minimal Inhibitory Concentrations (MIC) were determined against *Clostridium perfringens* ATCC13124 in Brain Heart Infusion broth supplemented with yeast extract (5 g/L) and hemin (5 mg/L) (BHI-YH) as described (2). MIC of untreated RumC1 was used to set the maximum of antimicrobial activity and calculate the residual activity of each treated RumC1. Stability and activity of RumC1 was also measured in physiological and higher concentration of salts: MIC of RumC1 was determined as above but the BHI-YH medium was replaced with Mueller Hinton (MH) broth supplemented in either NaCl at 100, 200, and 300 mM or in $MgCl_2$ at 1, 2 and 3 mM. For the stability to salts assays, MIC of untreated RumC1 in MH broth was used as the maximum of antimicrobial activity.

Simulated gastro-intestinal digestion of RumC1. RumC1 was treated with pepsin (Sigma-Aldrich) with a molecular ratio of 1:2.5 (RumC1:pepsin) at 37°C in sodium acetate 50 mM pH 2.5 for 2 hours with stirring (180 rpm) to mimic the digestive conditions occurring in the human stomach. To stop the enzymatic reaction of pepsin, $NaHCO_3$ 1M was added until pH 7 was reached. To simulate the intestinal compartment, RumC1 was incubated with pancreatin (Sigma-Aldrich) with a molecular ratio of 1:5 (RumC1:pancreatin) at 37°C in sodium acetate 50 mM pH 6.5 for 5 hours with stirring (180 rpm). Then Phenylmethanesulfonyl fluoride (PMSF, Sigma-Aldrich) was added to a final concentration of 0.1 mM to inhibit the action of pancreatin. MIC of treated RumC1 was determined against *C. perfringens* ATCC13124 in BHI-YH as described (2) after controlling that the enzymes in the above conditions without RumC1 showed no anti-*C. perfringens* activity. MIC of untreated RumC1 was used to set the maximum of antimicrobial activity and calculate the residual activity of each treated RumC1. Furthermore, RumC1 was detected by RP-C18-HPLC using an analytical column Jupiter 15-µm C18 300 Å (250 mm by 21.2 mm; Phenomenex). Elution was performed at 1 ml/min with a 0 to 40% linear gradient of 90% ACN and 0.1% TFA for 30 min. Finally, mass spectrometry analysis were conducted to compare the molecular masses of digested

RumC1 and untreated RumC1. As it has been reported that the bacteriocin nisin is digested by pancreatin but not by pepsin (13), nisin (from Sigma-Aldrich) was used as a positive control of the enzymatic activity of pancreatin only. To validate pepsin activity, Bovine Albumine Serum (BSA, Sigma-Aldrich) was used as a positive control.

Antimicrobial activity on human intestinal epithelium models. Caco-2 (ATCC HTB-37) and T84 (ATCC CCL-248) cells were being used as models of small intestinal and colonic epithelial cells, respectively. Cells were cultured in Dulbecco's modified essential medium (DMEM) supplemented with 10 % foetal calf serum (FCS), 1 % L-glutamine and 1 % Streptomycin-Penicillin antibiotics (all from Invitrogen). Cells were routinely seeded and grown onto 25 cm^2 flasks maintained in a 5 % CO_2 incubator at 37 °C. To test the influence of human intestinal epithelial cells on RumC1 activity, cells grown on 25 cm^2 flasks were detached using trypsin–EDTA solution (from Thermo Fisher Scientific), counted using Mallasez counting chamber and seeded into 96-well cell culture plates (Greiner bio-one) at approximately 10^4 cells per well. Cells were grown for 7-10 days until differentiation. The culture medium was then replaced twice with DMEM supplemented with 10% FCS but free of phenol red and of antibiotics 24h and 48h to make sure any trace of antibiotics was removed prior to the infection with *B. cereus.* A suspension of *B. cereus* DSM31 was prepared in the same media at a final concentration of 5.10^5 CFU/mL and added or not to Caco-2 and T84 monolayers. RumC1 was added 30 min before or at the same time or after the bacterial cells. Microplates were incubated for 24h at 37°C with 5% CO_2. Minimum inhibitory concentration (MIC) was defined as the lowest concentration of peptide that inhibited the growth of bacteria. Independent triplicate were made and sterility and growth controls were prepared for each assay.

MIC determination. Strains tested were acquired from commercial collections (the American Type Culture Collection (ATCC), www.atcc.org; the Collection de l'Institut Pasteur (CIP), www.pasteur.fr), from a laboratory collection (Centre National de Référence de la résistance aux antibiotiques, www.cnr-resistance-antibiotiques.fr) or from clinical sampling. *C. perfringens* CP24, 56, 60 were isolated from chickens and provided by UGent (14). Human clinical strains were mostly isolated from bloodstream infections, and in bone and joint infection at the University hospital of Besançon (France). The MIC were determined by broth microdilution for fastidious organisms (*Streptococcus pneumoniae*, *Listeria monocytogenes*, and *Bacillus cereus*), and non-fastidious organisms (*Enterococcus* species) by independent triplicates according to the EUCAST 2019 recommendations except for the Clostridia (15). Briefly, a bacterial suspension of Clostridia

was grown in anaerobic conditions (in a Trexler-type anaerobic chamber without stirring) and adjusted in MH broth supplemented with 5% lysed horse blood and 20 mg/L β-nicotinamide adenine dinucleotide at 5.10^6 UCF/mL. Ninety microliters of cell suspension were transferred in a sterile F-bottom polypropylene 96-well microplates. Thus, ten microliters of sterile RumC1 or antibiotics used as control from 100 to 0.1 µM by two-fold serial dilutions were added to the bacterial suspension to obtain a final concentration of 5.10^5 CFU/mL. Microplates were incubated 48h at 37°C in anaerobic conditions. MIC was defined as the lowest concentration of peptide that inhibited the growth of bacteria after 48h incubation at 37°C. Sterility and growth controls were prepared for each assay.

Macromolecules synthesis studies. *C. perfringens* ATCC 13124 was grown in BHI-YH broth (2) in airtight jars in the presence of anerobic atmosphere generation bags (Sigma-Aldrich) without stirring at 37°C until $OD_{600\ nm}$ reached 0.2. Then RumC1 or metronidazole or antibiotics with known mechanisms of action were added at 5xMIC. The antibiotics gemifloxacin, rifampicin, tetracycline and vancomycin were used as controls for the inhibition of DNA, RNA, protein and peptidoglycan synthesis, respectively. After 15 min of incubation at 37°C in anaerobic conditions, samples were labelled with [methyl-3H]thymidine or [5,6-3H]uridine or L-[4,5-3H(N)]-leucine or D-[1-3H] HCl glucosamine (all from Hartmann Analytic) at 10 µCi/mL to follow the synthesis of DNA, RNA, proteins and peptidoglycan respectively. After 45 min of incubation at 37°C in anaerobic conditions, bacterial cells were lysed and the macromolecules were precipitated with ice cold trichloroacetic acid (TCA, Sigma-Aldrich) at a final concentration of 20%; samples were kept on ice for an hour. Then the precipitates were filtered on Whatman glass microfiber filters pre-soaked in ice cold TCA 5%. After washing the filters with ice cold TCA 5% twice and then ice cold absolute ethanol once, they were soaked in 10 mL of scintillation liquid (Ultima Gold, PerkinElmer). Radioactivity was measured by liquid scintillation counting (TriCarb2800, PerkinElmer). As each condition displayed different growth rates, the radioactivity counts were normalized by the $OD_{600\ nm}$ of the samples. Results were expressed as a percentage of total macromolecule synthesis that was measured for each macromolecule with untreated cells. All experiments were done in independent triplicates.

ATP bioluminescent assays. *C. perfringens* ATCC 13124 was grown in BHI-YH broth (2) in anaerobic conditions (in a Trexler-type anaerobic chamber without stirring) at 37°C until $OD_{600\ nm}$ reached 0.4. Then *C. perfringens* cells were distributed in white polystyrene Nunc™ 96-well plate (ThermoFisher Scientific) and RumC1, metronidazole or nisin were added at 2.5, 5 or 10xMIC.

After 15 min of incubation in the same conditions, 100 µL of cells were mixed with 10 µL of luciferin-luciferase reagent (Yelen Analytics) prepared in IMI-Yelen Buffer (Yelen Analytics). The mix was homogenized and incubated 30 s before reading of the emitted photon using a microplate reader (Synergy Mx, BioTek). Then, 10 µL of lysis reagent (Yelen Analytics) was added to the mixture, homogenized and incubated 1 min before a new reading of the emitted photon. The intensity of the bioluminescent light was expressed as relative light units (RLU) which is proportional to extracellular ATP concentration (16). The inner ATP concentration was derived from the difference in ATP concentration in the extracellular media before and after cell lysis. Results were expressed as a percentage of total inner ATP concentration that was measured with untreated cells. All experiments were done in independent triplicates.

***Ex-vivo* evaluation of the RumC1 innocuity using human intestinal explants**. In order to evaluate the innocuity of RumC1 peptide for the human gut, *ex-vivo* experiments were performed using human explants as previously described (17). Human intestinal tissues, corresponding to ileocecal area, were obtained from patients undergoing surgery at the unit of gastrointestinal surgery, Hospital Laveran (Marseille, France), according to a collaborative "clinical transfer" project. The procedure was approved by the French ethic committee (CODECOH n° DC-2019-3402). All patients agreed for the use of their tissues for research purposes. Diagnoses leading to surgery were intestinal carcinoma. Samples were taken from macroscopically unaffected area as identified by the surgeons. After resection, the tissues were placed in ice-cold oxygenated sterile DMEM solution containing 1% (w/v) streptomycin/penicillin solution and 50 µg/mL gentamycin and were directly transferred to the laboratory within 15 min. Intestinal tissues were extensively washed and maintained in ice-cold culture media. Tissues were cleaned under binocular microscope from vascular vessels and conjunctive tissue using forceps. Intestinal explants (diameter of 0.5 cm^2) were then isolated from the cleaned resections using surgical punch, the complete procedure being complete in less than 2 h after the resections were obtained from the surgery unit. Finally, the explants were washed 3 times with culture media without antibiotics and transferred into 24-well plates before being incubated at 37°C during 4 h with RumC1 peptide diluted in DMEM media at 100 µM. In parallel, explants were left untreated (negative controls) or were incubated with the 300 µM of detergent cetyl trimethylammonium bromide (CTAB) used as positive control of tissue damages. After incubation, the explants were collected, washed three times with PBS^{2+} and fixed overnight at 4°C with PFA diluted at 4% (v/v) in PBS. The next day, intestinal explants were washed twice with PBS and included in inclusion medium (TFM - EMS), in transverse position to allow cutting respecting the crypt-villosity axis using cryostat (Leica CM3050). Four sections of 5

µm thickness were obtained per explant and each section being separated from the next by 100 µm in order to cover all the tissue. Explants were then stained using hematoxylin and eosin (H&E) staining protocol. Briefly, samples were incubated for 8 min in hematoxylin (from Sigma-Aldrich) and then allowed to stain by incubation with water for 2 min. Then explants were incubated for 1 min in eosin (from Sigma-Aldrich) and then in water for 1 min. This was followed by incubation of explants with ethanol at concentration of 70% then 95% and finally 100% for 2 min each. After blotting excess ethanol, intestinal explants were incubated for 15 min with xylene and mounted with coverslip using Eukitt mounting media (EMS, Hatfield, PA, USA). Finally, explants were left overnight to dry before examination of tissue organization under the microscope (Leitz DMRB microscope (Leïca) equipped with Leïca DFC 450C camera) (18).

SI References

1. B. H. Huynh, *et al.*, On the active sites of the [NiFe] hydrogenase from Desulfovibrio gigas. Mössbauer and redox-titration studies. *J. Biol. Chem.* **262**, 795–800 (1987).

2. S. Chiumento, *et al.*, Ruminococcin C, a promising antibiotic produced by a human gut symbiont. *Sci. Adv.* **5**, eaaw9969 (2019).

3. W. F. Vranken, *et al.*, The CCPN data model for NMR spectroscopy: development of a software pipeline. *Proteins* **59**, 687–696 (2005).

4. P. Güntert, C. Mumenthaler, K. Wüthrich, Torsion angle dynamics for NMR structure calculation with the new program DYANA. *J. Mol. Biol.* **273**, 283–298 (1997).

5. G. Cornilescu, F. Delaglio, A. Bax, Protein backbone angle restraints from searching a database for chemical shift and sequence homology. *J. Biomol. NMR* **13**, 289–302 (1999).

6. K. E. Kawulka, *et al.*, Structure of subtilosin A, a cyclic antimicrobial peptide from Bacillus subtilis with unusual sulfur to alpha-carbon cross-links: formation and reduction of alpha-thio-alpha-amino acid derivatives. *Biochemistry* **43**, 3385–3395 (2004).

7. C. S. Sit, M. J. van Belkum, R. T. McKay, R. W. Worobo, J. C. Vederas, The 3D Solution Structure of Thurincin H, a Bacteriocin with Four Sulfur to α-Carbon Crosslinks. *Angew. Chem. Int. Ed.* **50**, 8718–8721 (2011).

8. C. S. Sit, R. T. McKay, C. Hill, R. P. Ross, J. C. Vederas, The 3D structure of thuricin CD, a two-component bacteriocin with cysteine sulfur to α-carbon cross-links. *J. Am. Chem. Soc.* **133**, 7680–7683 (2011).

9. W. C. Chan, P. D. White, Eds., *Fmoc solid phase peptide synthesis: a practical approach* (Oxford University Press, 2000).

10. A. Janoschka, G. Svenconis, V. Schünemann, A closed cycle-cryostat for high-field Mössbauer spectroscopy. *J. Phys. Conf. Ser.* **217**, 012005 (2010).

11. H. P. Gunnlaugsson, Spreadsheet based analysis of Mössbauer spectra. *Hyperfine Interact.* **237**, 79 (2016).

12. V. Schünemann, H. Winkler, Structure and dynamics of biomolecules studied by Mössbauer spectroscopy. *Rep. Prog. Phys.* **63**, 263–353 (2000).

13. B. Jarvis, R. R. Mahoney, Inactivation of Nisin by Alpha-Chymotrypsin. *J. Dairy Sci.* **52**, 1448–1450 (1969).

14. A. R. Gholamiandekhordi, R. Ducatelle, M. Heyndrickx, F. Haesebrouck, F. Van Immerseel, Molecular and phenotypical characterization of Clostridium perfringens isolates from poultry flocks with different disease status. *Vet. Microbiol.* **113**, 143–152 (2006).

15. , v_9.0_Breakpoint_Tables.pdf (December 12, 2019).

16. E. W. Chappelle, G. V. Levin, Use of the firefly bioluminescent reaction for rapid detection and counting of bacteria. *Biochem. Med.* **2**, 41–52 (1968).

17. E. H. Ajandouz, *et al.*, Hydrolytic Fate of 3/15-Acetyldeoxynivalenol in Humans: Specific Deacetylation by the Small Intestine and Liver Revealed Using in Vitro and ex Vivo Approaches. *Toxins* **8** (2016).

18. H. Olleik, *et al.*, Temporin-SHa and Its Analogs as Potential Candidates for the Treatment of Helicobacter pylori. *Biomolecules* **9**, 598 (2019).